PERFORMANCE INVESTIGATION OF UWB RAKE RECEIVING AND TRANSMITTED REFERENCE SYSTEMS

by

Tao Jia

B.Eng., University of Science and Technology of China, 2003

A THESIS SUBMITTED IN PARTIAL FULFILLMENT
OF THE REQUIREMENTS FOR THE DEGREE OF

MASTER OF APPLIED SCIENCE

in the School
of
Engineering Science

© Tao Jia 2006

SIMON FRASER UNIVERSITY

Spring 2006

All rights reserved. This work may not be
reproduced in whole or in part, by photocopy
or other means, without the permission of the author.

APPROVAL

Name: Tao Jia

Degree: Master of Applied Science

Title of thesis: Performance Investigation of UWB Rake Receiving and Transmitted Reference Systems

Examining Committee: Dr. Andrew Rawicz
Chair

Dr. Dong In Kim, Senior Supervisor

Dr. Paul K. M. Ho, Supervisor

Dr. Daniel C. Lee, Examiner

Date Approved: Mar. 30/06

SIMON FRASER UNIVERSITY library

DECLARATION OF PARTIAL COPYRIGHT LICENCE

The author, whose copyright is declared on the title page of this work, has granted to Simon Fraser University the right to lend this thesis, project or extended essay to users of the Simon Fraser University Library, and to make partial or single copies only for such users or in response to a request from the library of any other university, or other educational institution, on its own behalf or for one of its users.

The author has further granted permission to Simon Fraser University to keep or make a digital copy for use in its circulating collection, and, without changing the content, to translate the thesis/project or extended essays, if technically possible, to any medium or format for the purpose of preservation of the digital work.

The author has further agreed that permission for multiple copying of this work for scholarly purposes may be granted by either the author or the Dean of Graduate Studies.

It is understood that copying or publication of this work for financial gain shall not be allowed without the author's written permission.

Permission for public performance, or limited permission for private scholarly use, of any multimedia materials forming part of this work, may have been granted by the author. This information may be found on the separately catalogued multimedia material and in the signed Partial Copyright Licence.

The original Partial Copyright Licence attesting to these terms, and signed by this author, may be found in the original bound copy of this work, retained in the Simon Fraser University Archive.

Simon Fraser University Library
Burnaby, BC, Canada

Abstract

This thesis investigates the performances of the Rake receiving and the Transmitted Reference (TR) schemes for Ultra Wideband (UWB) communication systems. UWB technology has been proposed as a promising physical layer candidate for indoor wireless communications, because it offers very fine time resolution and multipath resolvability. However, these beneficial properties also pose great challenges to the design of a low-complexity UWB receiver.

In this thesis, we first develop a theoretical framework to precisely analyze the performance of the UWB Rake receiving and TR systems in realistic indoor environments. We also demonstrate how the TR scheme achieves a low-complexity receiver implementation at the expense of certain performance degradation and information rate loss. To overcome these, we propose a novel UWB-TR scheme, namely M-ary orthogonal coded/Balanced TR system. Our results show that the proposed balanced TR scheme outperforms the conventional TR schemes with slightly increased transceiver complexity.

Keywords: Ultra Wideband (UWB), Rake receiver, Transmitted Reference (TR).

To my parents
for their constant support

Acknowledgments

I offer my enduring gratitude to the faculty, staff and fellow students in the school of Engineering Science, who have created an excellent environment for my master studies. I especially thank my senior supervisor, Dr. Dong In Kim, for all the guidance and support in the past two years. I have benefited tremendously from his unique blend of energy, vision and technical insights. I also express my great thanks to my supervisor, Dr. Paul Ho, for being a great teacher. His courses have well prepared me for carrying out this thesis work. I thank my thesis examiner, Dr. Daniel Lee, for acting as my thesis committee member and bringing questions.

I feel fortune to work with my colleagues in RF/Microwave Mobile Communications Laboratory. I benefited much from many stimulating discussions with Serhat Erküçük. I also express my gratitude to Mike and Brad for being good friends and all their helps in these two years. I thank Sara, Shirin, Wan Jong, Ted and other people who have combined to create a good working place.

I owe special thanks to my girl friend, Xiaoxing Li, for her supports and encouragements in my everyday's life in Canada. Finally, I am deeply indebted to my parents for their constant supports throughout my life, especially my father, who has passed way and can not see my graduation.

Contents

Approval ii

Abstract iii

Dedication iv

Acknowledgments v

Contents vi

List of Tables ix

List of Figures x

List of Abbreviations xii

1 Introduction 1

1.1 Introduction 1

1.2 Contributions and Organization of the thesis 5

2 Background 7

2.1 A Short History of UWB Technology 7

2.2 UWB Transmission 8

2.3 UWB Channel Models 10

3 UWB Rake and TR Systems 15

3.1 UWB Rake Reception 15

3.1.1 System Model 16

3.1.2 Rake Performance Analysis 18
3.2 UWB-TR system 22
3.2.1 System Model 23
3.2.2 Single-user UWB-TR system 24
3.2.3 Multiuser UWB-TR system 25
3.3 Performance Results 26
3.4 Conclusion 34

4 M-ary Orthogonal Coded/Balanced TR UWB system 36
4.1 Hybrid Matched Filter Correlator UWB-TR receiver 37
4.2 M-ary Orthogonal Coded/Balanced UWB-TR system 37
4.2.1 Transmitter 38
4.2.2 Receiver 40
4.2.3 The IPI cancellation 41
4.3 Performance Analysis 44
4.3.1 Derivation of SER 44
4.3.2 Timing jitter 48
4.4 Performance Results 50
4.5 Conclusion 56

5 Conclusions and Future works 57
5.1 Conclusions 57
5.2 Future works 58

Appendices 60

A 60
A.1 Evaluation of $P_q^{(n)}$ 60
A.2 Evaluation of average path energy $\mathbf{E}\{{A_n^{(\nu)}}^2\}$ 61
A.3 SNR and SINR for UWB-TR systems 62
A.3.1 Average SNR for single-user UWB-TR system 62
A.3.2 Average SINR for multiuser UWB-TR system 64

B **65**

B.1 Evaluation of σ_1^2 in (4.21) 65

B.2 Evaluation of $\sigma_{2,k}^2$ in (4.24) 66

B.3 Evaluation of μ_k and $\sigma_{\xi_{k,\varepsilon}}^2$ in (4.28) and (4.29) 67

Bibliography **69**

List of Tables

2.1 UWB channel model parameters and main characteristics 13

3.1 Average total channel energy for indoor UWB channel models. 26

4.1 Information rate increase offered by $M = 2$-ary/Balanced TR system relative to the conventional TR whose delay T_d varies from $2T_c$ to $T_m = 200T_c$ (target BER 10^{-2}). 55

List of Figures

2.1 UWB pulse waveform in (a) time domain; (b) frequency domain 8
2.2 FCC spectral mask and Part 15 limits 9
2.3 Typical received UWB signals in (a) CM1; (b) CM3 14

3.1 TR receiver. 23
3.2 Average output SINR versus the number of Rake fingers Q for CM1, CM2 when $E_b/N_o = 20$dB. 27
3.3 Average output SINR versus the number of Rake fingers Q for CM3, CM4 when $E_b/N_o = 20$dB. 28
3.4 Average output SNR versus the integration interval for CM1, CM2 when $E_b/N_o = 20$dB. 29
3.5 Average output SNR versus the integration interval for CM3, CM4 when $E_b/N_o = 20$dB. 30
3.6 Optimum integration interval versus E_b/N_o for 4 different types of channel models CM1 to CM4. 31
3.7 BER performance versus E_b/N_o with adaptively selected integration intervals for CM2 and CM4. 32
3.8 Average output SINR versus number of users for varying E_b/N_o for CM1. . . 33
3.9 Optimum integration interval versus E_b/N_o for CM1 and CM3 under the multiuser scenario. 34

4.1 Hybrid matched filter correlation TR receiver structure. 37
4.2 M-ary orthogonal coded/Balanced TR system: the transmitter. 39
4.3 M-ary orthogonal coded/Balanced TR system: the receiver. 41
4.4 the IPI cancellation mechanism of the proposed system. 42

4.5 (a), (b) are the received waveforms; (c), (d) are the correlator inputs; for the conventional and the proposed TR systems, respectively 43
4.6 SER versus per-bit SNR for the M-ary/Balanced TR system. 50
4.7 SER degradation with timing jitters for the M-ary/Balanced TR systems, when $T_d = 16$ chips. 51
4.8 BER versus per-bit SNR for the M-ary/balanced TR, balanced TR and the conventional TR systems, when $T_d = 16$ chips. 52
4.9 BER versus per-bit SNR for the conventional and M-ary/Balanced TR systems with respect to T_d, for $N_s = 4\,(M = 2)$, when there is no timing jitter. . 53
4.10 BER versus per-bit SNR for the conventional and M-ary/Balanced TR systems with respect to T_d, for $N_s = 4\,(M = 2)$, when there exists 10% timing jitter. 54

A.1 One possible channel realization for nth time bin in the discrete-time channel model. 61

List of Abbreviations

UWB	Ultra wideband
IR	Impulse radio
TH	Time hopping
PPM	Pulse position modulation
PAM	Pulse amplitude modulation
MAI	Multiple access interference
TR	Transmitted reference
WLAN	Wireless local area network
WPAN	Wireless personal area network
CDMA	Code division multiple access
OFDM	Orthogonal frequency division multiplexing
AcR	Autocorrelation receiver
GLRT	Generalized likelihood ratio test
IPI	Inter-pulse interference
IFI	Inter-frame interference
BER	Bit-error rate
SER	Symbol-error rate
SINR	Signal-to-interference-plus-noise ratio
SNR	Signal-to-noise ratio
LTI	Linear time-invariant
PDP	Power delay profile
MPC	Multipath component
LOS	Line-of-sight
NLOS	non-line-of-sight

AWGN	Additive white Gaussian noise
CF	Characteristic function
pdf	Probability density function
PDF	Probability distribution function
MRC	Maximum ratio combining

Chapter 1

Introduction

1.1 Introduction

Modern wireless technology has the potential to change the way people or devices communicate with each other. With the wireless convenience introduced by the widely use of cell phones and mobile PCs, people will soon demand the same wireless connectivity throughout their digital home, connecting PCs, digital cameras, camcorders and other storage devices as a wireless personal area network (WPAN). However, existing WPAN and wireless local area network (WLAN) technologies, e.g. Bluetooth and Wi-Fi, can not meet the requirements for supporting multiple high-speed indoor communications in a cost effetive way.

Ultra Wideband (UWB), or impulse radio (IR) technology, on the other hand, has been proposed as a promising physical layer candidate for indoor short-range high-rate wireless communications [1]-[3]. Compared to the existing narrowband technologies, UWB has several unique advantages. First of all, it does not use a sinusoidal carrier to raise the signal to the radio frequency (RF) band, which means a UWB radio may be manufactured inexpensively. In fact, the techniques and devices for generating UWB signals have existed for more than thirty years and are well known to radar community. Secondly, by the transmission of short-duration pulses with a pulse width on the order of sub-nanoseconds, UWB signals offer very fine time resolution and multipath resolvability. Specifically, the extremely-wide bandwidth occupancy from near dc to a few gigahertz means that the multipath resolution is down to path differential delays less than a nanosecond, or equivalently down to path length differential delays less than a foot, which greatly reduces the severe multipath fading effects in indoor environments [4]. Consequently, when designing a UWB system, the fading

margin in link budgets can be significantly reduced, which allows for low transmit power operations. Another power saving effect stems from the fact that the transmission and reception of UWB signals are low duty cycle (less than 0.5 percent). Although the peak or instantaneous power can be relatively large, the average power becomes considerably lower. As a result, UWB radios will have longer battery life. Last but not the least, since UWB devices operate at a power level as low as the background noise, they will less likely interfere with the existing narrowband systems.

A simple comparison between UWB and existing narrowband technologies clearly illustrates its unique suitability for short-range high-speed communications, using the merit *spatial capacity* (bits/s/m^2) as in [25]. Existing WLAN/WPAN technologies operate at the 2.4-GHz industrial, scientific and medical (ISM) band which contains 80 MHz free spectrum. For WLAN, three 22-MHz IEEE 802.11b systems can be supported simultaneously without interfering each other, resulting in a peak rate of 11 Mbps for an aggregate rate of 33 Mbps[1]. With an operating range of 100-m for WLAN, this yields a spatial capacity of approximately 1 Kb/s/m^2. Bluetooth has an operating range of 10-m and a peak rate of 1 Mpbs. Studies show that approximately ten Bluetooth clusters can operate simultaneously in this range with minimal degradation, yielding an aggregate rate of 10 Mpbs. This translates to a spatial capacity of about 30 Kb/s/m^2. UWB systems, on the other hand, are designed for 110 Mbps at a 10-m operating range with four co-existing clusters, which leads to a spatial capacity of about 1.3 Mb/s/m^2. As can be easily seen, UWB offers much higher data intensity.

However, the potential benefits promised by UWB technology also pose great challenges to the design of low-cost and low-complexity UWB communication systems. Experimental results have shown that in typical indoor environments, the maximum channel delay spreads of 60-70 ns are observed. This implies that, by transmitting sub-nanosecond pulses, the signal energy will be spreaded over a large number of multipath components (MPCs). To fully collect the signal energy, a commonly-used Rake receiver has to implement tens or even hundreds of correlation branches [5]. On the other hand, the receiver using only a single correlator may operate at a signal energy 10-15 dB lower than a full Rake receiver [6, 7]. This has become one of the most limiting factors in designing a UWB Rake receiver with manageable complexity. In addition, to combine the signal energy from all MPCs in

[1]Even with IEEE 802.11a or 802.11g, which offer 54 Mbps peak rate, the resulting data intensity is still lower than that in UWB system.

a coherent way, precise channel estimation has to be achieved. This further increases the receiver complexity, especially when the number of MPCs is large. Moreover, for the Rake receiver, stringent timing requirements are required for individual pulse correlation branch, which means the system performance is sensitive to the timing jitter [30].

For the above reasons, much attention has been drawn to the UWB transmitted reference (UWB-TR) scheme. The original idea of transmitted reference scheme dates back to the 1960s [8, 9], and was firstly applied to UWB systems in [10]. In UWB-TR system, the transmitter sends pairs of pulses, each consisting of a reference pulse and a data-modulated pulse. The receiver correlates the received reference signal with the data signal to collect the multipath-spreaded signal energy. In this way, the reference pulse provides an immediate channel estimation for the detection of its associated data pulse. In order for the two pulses to experience the same channel condition, the separation between the two pulses has to be within the channel coherence time. The UWB-TR system has several advantages over the Rake receiving system in terms of implementation complexity. First, it simply needs an autocorrelation receiver (AcR) in stead of many Rake fingers to capture the multipath energy. Second, it does not require the channel estimation, thus is not sensitive to the channel estimation errors that may deteriorate the performance of Rake receivers. In addition, in stead of requiring timing synchronization for each Rake finger, the TR scheme only needs synchronization for one correlation operation. However, the simplicity of the UWB-TR system is achieved at the expense of certain amount of performance degradation. Simply put, it wastes power and time to transmit the reference pulses, which *effectively* degrades the detection performance and sacrifices the information rate. Moreover, because a *noisy* reference is used as the template signal for correlation, the noise effect is enhanced by introducing an additional noise-times-noise term, which further degrades the detection performance.

Regardless of its drawbacks, UWB-TR scheme is still appealing as long as the receiver complexity is of greater concern. Indeed, there have been many proposals on improving the detection performance and/or increasing the information rate for UWB-TR systems [11]-[20]. To improve the detection performance, most approaches focus on obtaining a cleaner template by averaging multiple reference pulses prior to the cross-corrleation [11, 13, 16]. Because the noise components corrupting these reference pulses are added in a non-coherent way, the noise effect can be reduced by a factor equal to the number of the reference pulses being averaged. Furthermore, [13] has derived the optimal TR receiver structure based on

a generalized likelihood ratio test (GLRT) and analyzed its performance. In addition, the authors in [13] also proposed a differential TR system, which outperforms the standard TR system. However, differential TR may require more than a symbol time delay for random time-hopping shift, which may not be feasible at the current time. The performance results in [13] have also suggested that averaging multiple reference pulses prior to the cross correlation is a good tradeoff between the performance and the receiver complexity. Notable in [16], the authors have proposed a hybrid matched filter correlator UWB-TR receiver structure, which not only realizes the reference averaging, but also enables the receiver to operate at the symbol-rate rather than the TR system operating at the *frame-rate* as in [11] and [13]. The benefits resulted from this rate reduction are obvious, e.g., reducing the system's sampling frequency and the power consumption required by the post-processing. On the other hand, to increase the information rate, there is one proposal [18] on optimizing the number of and the power allocation for the reference pulses, or pilot waveforms as called therein, to minimize the time and the power loss for transmitting the reference signals. However, in these UWB-TR systems, one assumption has always been made, i.e., the distance between the reference and the data pulses is set to be at least equal to the maximum channel delay spread, resulting in no inter-pulse interference (IPI) between the reference and the data signals even after transmitting through the multipath channel. Considering that the channel delay spreads for UWB signals are as large as about 60-70 ns and the pulse width is usually on the order of sub-nanosecond, this assumption exerts a stringent limit on the UWB-TR system's achievable information rate. Therefore, releasing this restriction is necessary, especially for high-data-rate UWB communications. In [19], the authors proposed a maximum likelihood template estimator and analyzed its performance in the presence of IPI. However, in this proposal, the IPI is suppressed in a *statistical* way and the complexity associated with the maximum likelihood estimation as well as storing multiple symbol waveforms is prohibitively high. Consequently, there exists a need for a low-complexity UWB-TR system that is not subject to the IPI and more suitable for indoor high-data-rate UWB communications.

In this thesis, rather than directly jumping into the UWB-TR system design, we start with developing a theoretical framework to analyze the performance of the UWB Rake receiver, in terms of its channel-averaged output signal-to-interference-plus-noise ratio (SINR). Compared to the existing works regarding the performance analysis for the UWB Rake receiver, our work gives a pure analytical result, rather than the semi-analytical/experimental

or semi-analytical/simulation approaches, for the channel-averaged output SINR. Note that this theoretical framework is also applicable to the UWB-TR system. In [12, 14], the authors have addressed the issues of the optimal integration interval for the UWB-TR system and presented performance results based on that. However, the optimal integration interval therein is determined by simulation. In addition, it is found in a single-user communication scenario and may no longer be optimal in a multiuser communication environment. In this thesis, we demonstrate that our framwork can be used to *analytically* determine the optimal integration interval for UWB-TR system, even in a multiuser scenario. After that, to the best of our efforts, we have attempted to derive a close-form expression for the channel-averaged bit-error-rate (BER). However, we found that, without affecting the essence of the indoor UWB channel model, the derivation of a close-form BER expression is unwieldy. Another purpose for carrying out this analysis is to give some performance comparisons between the UWB Rake receiving and the UWB-TR systems, thus show the necessities of improving the performances for UWB-TR systems. For that, we propose a novel UWB-TR signaling scheme, namely M-ary orthogonal coded/Balanced TR system, by designing the transmitter and the receiver in a joint manner. The major characteristic of the proposed scheme is that it can fully eliminate the IPI in a *deterministic* way. As a result, the distance between the reference and the data pulses can be reduced to a minimum value (for the increased information rate) without causing any performance degradations. Besides, an M-ary orthogonal modulation scheme is introduced to further increase the information rate. Compared to the previous UWB-TR schemes which do not consider the IPI, our proposed scheme can operate at higher information rates, while maintaining its superior BER performance with even lower transmit power. Compared to the previous approach dealing with the IPI, our scheme achieves the *complete* cancellation of the IPI with a lower receiver complexity, while offering some additional information rate increase. It is to be understood that, as most other TR system designs, there are some implementation issues associated with our scheme and they will be discussed in this thesis as well.

1.2 Contributions and Organization of the thesis

Compared with the existing works, this thesis has the following main contributions:

- Developed a theoretical framework to analyze the performance of the UWB Rake receiving and UWB-TR systems, in terms of their channel-averaged output SINRs.

- Proposed a novel UWB-TR signaling scheme which fully eliminates the IPI between the reference and data pulses, thus significantly increases the UWB-TR system's achievable information rate. A detailed performance analysis of the proposed system and its information rate increase compared to the standard UWB-TR system are also given.

The remainder of this thesis is organized in the following way. In Chapter 2, we provide some background information about UWB communications. We will also introduce the newly-accepted IEEE 802.15.3a indoor wireless channel models for high-data-rate UWB communications. In Chapter 3, we develope the abovementioned theoretical framework for the SINR analysis and give some basic performance comparisons between the UWB Rake receiving and the UWB-TR system. In Chapter 4, we describe the transceiver structure of our proposed UWB-TR system, followed by a detailed performance analysis as well as some simulation results. Finally, we draw the conclusions and address some future research issues in Chapter 5.

Chapter 2

Background

2.1 A Short History of UWB Technology

UWB technology originated from the early works on time-domain electromagnetics back in 1962 [24]. It was firstly used to characterize the transient behavior of a certain class of microwave networks, by measuring their impulse responses $h(t)$. It is well known that the output $y(t)$ of a linear, time-invariant (LTI) system to any input $x(t)$ can be uniquely determined by

$$y(t) = \int_{-\infty}^{+\infty} h(\tau)x(t-\tau)d\tau. \tag{2.1}$$

With the advent of the sampling oscilloscope and the development of techniques for sub-nanosecond pulse generation, to approximate an impulse excitation, the direct measurement of the impulse response $h(t)$ based on (2.1) became feasible. Soon, the same techniques for generating and measuring short pulses were used to develope radar and communication systems, usually referred to as *baseband*, *carrierless* or *impulse* communications. It was not until approximately 1989 that the U.S. Department of Defense coined the term "ultra wideband". By that time, UWB theories and techniques have experienced nearly 30 years of extensive development. Within the United States, the development of UWB technology has been greatly accelerated since its classification restrictions were removed in 1994. In the academic context, Prof. Robert A. Scholtz and his research group pioneered applying UWB technology to the multiple access communications in the early 1990s. From then on, the most recent 10 years' development of UWB technology has particularly witnessed the great attention it has drawn from both academic and industrial communities.

2.2 UWB Transmission

UWB technology is at present defined by the Federal Communications Commission (FCC) as any wireless transmission scheme which occupies a fractional bandwidth of 20% or greater, or an absolute bandwidth of more than 500 MHz, where the fractional bandwidth is defined by [26]

$$\text{Fractional Bandwidth} = \frac{B}{f_c} \tag{2.2}$$

where $B = f_H - f_L$ is the -10 dB bandwidth and $f_c = (f_H + f_L)/2$ is the center frequency, with f_H and f_L denoting the upper and lower -10 dB emission points, respectively.

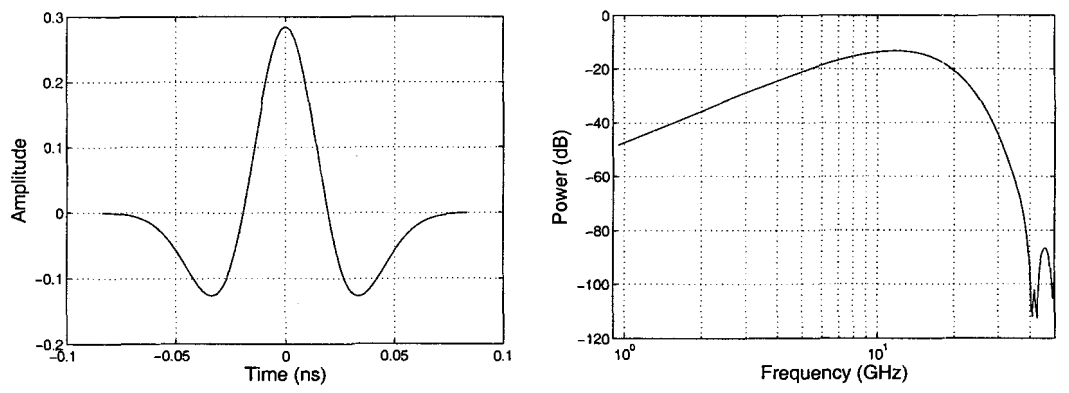

(a) (b)

Figure 2.1: UWB pulse waveform in (a) time domain; (b) frequency domain

In traditional pulse-based UWB systems, such large bandwidth is achieved by transmitting extremely short-duration pulses, usually with a pulse width on the order of sub-nanoseconds. The transmission is in baseband, i.e., no sinusoid carrier is needed, and the resulting bandwidth spans from dc to a few gigahertz. Generally, the Gaussian monocycles obtained by differentiating the standard Gaussian pulse have been extensively used for the analytical and simulation purposes. Fig. 2.1 shows such an ideally (no distortion) received pulse waveform(together with its Fourier transform in frequency domain), which is

the second-order derivative of a Gaussian pulse[1], given by

$$w_{\text{rec}}(t) = \left[1 - 4\pi(t/\tau_m)^2\right] \exp\left[-2\pi(t/\tau_m)^2\right], \tag{2.3}$$

where τ_m is a parameter related to the pulse width.

The carrierless transmission implies that a UWB transmitter can be manufactured less expensively compared to the narrowband devices. On the other hand, its signal energy distributed over the frequency bands dedicated for the existing narrowband radio systems, e.g., WLAN and Bluetooth, may deteriorate the performances of these systems. As a result, the FCC announced the first Report and Order (R&O) in Februrary 2002, which permits the unlicensed deployment of UWB devices in the 3.1-10.6 GHz band by conforming to the spectral mask defined by FCC Part 15 rules [27], as shown in Fig. 2.2. It can be easily

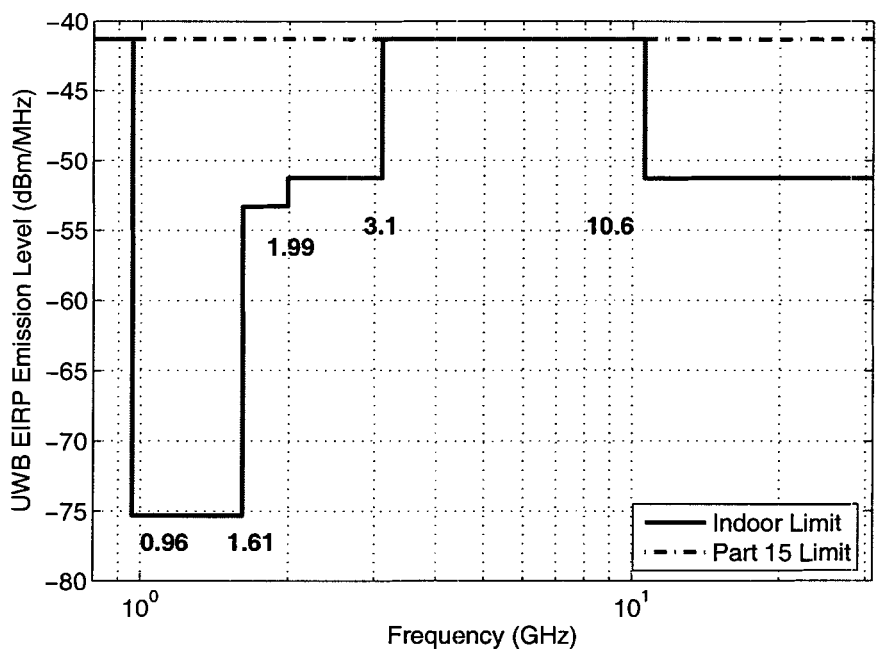

Figure 2.2: FCC spectral mask and Part 15 limits

observed that the pulse waveform shown in Fig. 2.1 does not meet the spectral mask set by the FCC. Therefore, there have been many proposals on modifying the pulse shape to

[1]Generally, both the transmitter and the receiver antennas act as differentiator.

meet this spectrum requirements, e.g., [28] and [29]. However, pulse design is not the main concern of this thesis and does not affect the main results we have reached here. Thus, as in most existing works, we will use the originally proposed Gaussian monocycles for both analyses and simulations.

Besides the traditional pulse-based UWB radio system, there is an alternative scheme, namely multiband UWB. Rather than utilizing the entire 3.1-10.6 GHz band simultaneously, multiband UWB scheme divides the whole band into several (typically 3-10) subbands and transmits the information on each band. The detailed comparison between the two systems is beyond the scope of our research. In this thesis, we only consider the pulse-based UWB and will simply refer to it as UWB hereafter.

In UWB communication systems, there are mainly two types of modulation methods, pulse position modulation (PPM) and pulse amplitude modulation (PAM). In PPM, each symbol duration is divided into several frames. In each frame, only one pulse is transmitted. The information bit is encoded by the positions of the pulses in those frames. In PAM, the signaling format is essentially same as in PPM except that the information bit is represented by the amplitudes of the pulses. Without loss of generality, we will only consider binary PPM (BPPM) and binary PAM (BPAM) in this thesis. Note that BPAM is equivalent to bi-polar or antipodal modulation. To be more consistent with existing works, we have considered BPPM for UWB Rake receiving system and BPAM for TR systems.

To allow for the multiple access, two approaches have been proposed, time-hopping (TH) [1, 2, 3] and direct sequence (DS) [32]. In TH-UWB systems, each user is assigned a unique pseudo-random sequence, which determines an additional time shift onto the pulse position within each frame, in order to avoid the catastrophic collisions among different users. In DS-UWB systems, rather than sending one pulse per frame as in TH-UWB systems, each symbol is represented by a series of consecutive pulses which are pulse-amplitude modulated by a user-specific spreading sequence. In this thesis, we only consider the more classical TH-UWB systems.

2.3 UWB Channel Models

Wireless propagation channels have been intensively studied for nearly five decades. Generally speaking, the signal after propagating through wireless channels consists of multiple replicas of the originally transmitted signal. These replicas, called multipath components

(MPCs), can be characterized by their arrival times and attenuations. In traditional channel models for the narrowband systems, the most widely adopted channel model is flat Rayleigh fading channel. The assumption of flat fading is valid only when the system bandwidth is very small, where the delays of MPCs at the receiver can be ignored. In addition, all the MPCs arrived at the receiver are added constructively or destructively. If the number of MPCs is large, the combined channel gain coefficient will be a complex Gaussian random variable, yielding a Rayleigh amplitude distribution. In cellular systems, the bandwidth occupancy has been increased to around 20 MHz. In this case, the wireless channels exhibit frequency selectivity, which means the signals at different frequency ranges experience different attenuations. Back to the time domain, this translates to the fact that the MPCs arrived at the receiver with different delays will have different powers. The power delay profile (PDP) describes how the power is distributed among different MPCs corresponding to their delays. Usually, it is modeled by the average signal power within certain delay time bin interval, which is approximately the inverse of the system bandwidth. In cellular systems, the number of MPCs arrived in each time bin is usually large enough to validate the central limit theorem. Hence, the amplitude distribution can be still modeled as Rayleigh.

However, in UWB systems, the bandwidth has been increased to about 7.5 GHz, for which the wireless channels will be highly frequency-selective. The immediate result from this extremely-wide bandwidth occupancy is the system's resolvable time bin is on the order of sub-nanoseconds. In each of such small time bins, only a few MPCs arrive and the central limit theorem is no longer applicable. Consequently, it is necessary to develop an appropriate wireless channel model to facilitate the physical layer analysis for UWB systems. Indeed, there have been many measurement campaigns for the UWB propagation channels in the past few years.

In 2002, the IEEE 802.15.3a task group released an indoor wireless channel model for high-data-rate UWB communications, for the purpose of making fair comparisons between different physical layer proposals. Compared to the existing narrowband channel models, the MPCs in this channel model arrive in a clustered manner. Specifically, the arrival times of the clusters are Poisson distributed. Within each cluster, there are a number of MPCs, called rays, and the arrival times of these rays are also Poisson distributed. The channel gain coefficient of each MPC has an independent lognormal distribution. Furthermore, a double-exponential model is found to be best fit for the PDP. To be more specific, the

continuous-time impulse response of this UWB channel model can be written as [33]

$$h(t) = \sum_{l=0}^{L} \sum_{k=0}^{K} \alpha_{k,l}\, \delta(t - T_l - \tau_{k,l}) \tag{2.4}$$

where the associated parameters are defined as follows:

- T_l is the arrival time of the lth cluster
- $\tau_{k,l}$ is the arrival time of the kth ray within the lth cluster. Note that $\tau_{0,l} = 0$
- $\alpha_{k,l}$ is the gain coefficient of the kth ray in the lth cluster.
- $\delta(\cdot)$ is the direc delta function

The inter-cluster and inter-ray arrival times are independently exponentially distributed, given by

$$P(T_l|T_{l-1}) = \Lambda \exp\left[-\Lambda(T_l - T_{l-1})\right], \quad l > 0, \tag{2.5}$$

$$P(\tau_{k,l}|\tau_{k-1,l}) = \lambda \exp\left[-\lambda(\tau_{k,l} - \tau_{k-1,l})\right], \quad k > 0. \tag{2.6}$$

where $P(\cdot)$ denotes the probability distribution function and $\{\Lambda, \lambda\}$ are the arrival rates of the clusters and the rays, respectively. The channel gain coefficient $\alpha_{k,l} = p_{k,l}\xi_l\beta_{k,l}$, where $p_{k,l}$ equiprobably takes on the values of ± 1 accounting for the random pulse inversion that occurs due to pulse reflections and $\xi_l\beta_{k,l}$ is a lognormal random variable, denoted by

$$20\log_{10}(\xi_l\beta_{k,l}) \propto \text{Normal}(\mu_{k,l}, \sigma_1^2 + \sigma_2^2) \tag{2.7}$$

In (2.7), ξ_l and $\beta_{k,l}$ represent the lognormal fadings associated with the lth cluster and the kth ray of the lth cluster, respectively. Because they are both lognormal random variables, the product of them again is a lognormal random variable. σ_1 and σ_2 correspond to the fadings of the clusters and the rays, respectively. Furthermore, the PDP is double exponentially decaying, given by

$$\mathbf{E}\{|\xi_l\beta_{k,l}|^2\} = \Omega_0 \exp(-T_l/\Gamma) \exp(-\tau_{k,l}/\gamma) \tag{2.8}$$

where $\mathbf{E}$ denotes the expectation. Ω_0 is the mean power of the first ray of the first cluster, Γ and γ represent the power decay factors of the clusters and the rays, respectively. The $\mu_{k,l}$ is thus given by

$$\mu_{k,l} = \frac{10\ln\Omega_0 - 10T_l/\Gamma - 10\tau_{k,l}/\gamma}{\ln 10} - \frac{(\sigma_1^2 + \sigma_2^2)\ln 10}{20} \tag{2.9}$$

Also note that the path loss model and the shadowing effect have not been included here. In other words, we focus more on the small scale fading.

In summary, one set of parameters $\{\Lambda, \lambda, \Gamma, \gamma, \sigma_1, \sigma_2\}$ determines the statistical behavior of the wireless channel. Based on the measurements that have been made, the IEEE 802.15.3a task group defined the following four types of indoor wireless channel models, shown in Table 2.1 [33].

Table 2.1: UWB channel model parameters and main characteristics

Target channel characteristics	**CM1**	**CM2**	**CM3**	**CM4**
Mean delay spread (ns)	5.05	10.38	14.18	
RMS delay spread (ns)	5.28	8.03	14.28	25
NP 10dB			35	
NP (85%)	24	36.1	61.54	123.3
Model parameters				
Λ(1/ns)	0.0233	0.4	0.0677	0.0677
λ(1/ns)	2.5	0.5	2.1	2.1
Γ(s)	7.1	5.5	14.0	24.0
γ(s)	4.3	6.7	7.9	12
σ_1(dB)	3.4	3.4	3.4	3.4
σ_2(dB)	3.4	3.4	3.4	3.4
Model characteristics				
Mean delay spread (ns)	5.0	9.9	15.9	30.1
RMS delay spread (ns)	5.0	8.0	15.0	25.0
NP 10dB	12.5	15.3	24.9	41.2
NP (85%)	20.8	33.9	64.7	123.3

In Table 2.1, CM1 corresponds to a line-of-sight (LOS) channel measurement with a transceiver separation of 0-4 m. CM2 and CM3 are based on non-line-of-sight (NLOS) channel measurements with transceiver separations of 0-4 m and 4-10 m, respectively. CM4 is to fit a 25 ns RMS delay spread to represent an extreme NLOS multipath channel. NP 10dB denotes the number of MPCs within 10dB of the strongest MPC and NP 85% denotes the number of MPCs that captures 85% of the total channel energy. Note that the definitions of the mean delay spread and RMS delay spread can be found in [35].

The model characteristics in Table 2.1 show that UWB indoor wireless channel models have large channel delay spreads and the signal energy is spreaded over a large number of

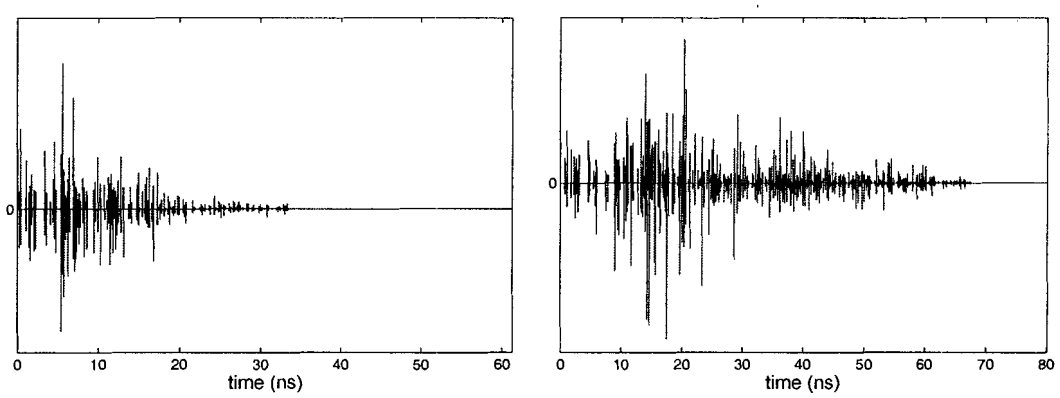

(a) (b)

Figure 2.3: Typical received UWB signals in (a) CM1; (b) CM3

MPCs. In Fig. 2.3, we plot typical received UWB signals after transmitting a single pulse through CM1 and CM3, respectively. As can been seen, the received signals spread over 30 ns and 60 ns in CM1 and CM3, respectively. Hence, how to efficiently collect the signal energy with manageable receiver complexity becomes a crucial task to the UWB system designers and engineers.

Chapter 3

UWB Rake and TR Systems

In this chapter, we develop a theoretical framework to analyze the performances of UWB Rake receiving and TR systems, in terms of their channel-averaged output SINRs. We will also present some performance comparisons between the two systems and demonstrate how the UWB-TR system achieves reduced receiver complexity at the expense of some performance degradations. The materials in this chapter have been published in [15][1].

3.1 UWB Rake Reception

Since the original proposal of time-hopping (TH) impulse radio by [1], there have been a number of researches attempting to analyze the exact performance of UWB systems. In [21], the authors derived an exact BER expression using the characteristic function (CF) method and evaluated the accuracy of the Gaussian approximation of MAI used in [1, 2, 3]. However, they only examined the system performance based on a simple additive white Gaussian noise (AWGN) channel model, rather than a realistic indoor multipath channel model. On the other hand, the authors in [7] presented SNR and BER performances for different UWB Rake receivers, based on the newly-accepted IEEE 802.15.3a UWB indoor wireless channel models.

[1] © 2005 IEEE. Reprinted, with permission, from *Proc. IEEE VTC Spring'05*, vol. 2, pp. 1396–1400, Stockholm, Sweden, May 2005.

This material is posted here with permission of the IEEE. Such permission of the IEEE does not in any way imply IEEE endorsement of any of Simon Fraser University (SFU)'s [Library & Archives Canada's] products or services. Internal or personal use of this material is permitted. However, permission to reprint/republish this material for advertising or promotional purposes or for creating new collective works for resale or redistribution must be obtained from the IEEE by writing to pubs-permissions@ieee.org. By choosing to view this document, you agree to all provisions of the copyright laws protecting it.

However, only the single-user scenario has been considered. Besides, the results are given in a semi-analytical way. By that time, as long as the IEEE 802.15.3a UWB channel model is concerned, there is not any pure analytical work available which is capable of directly evaluating the system performances. Although the theoretical framework we have developed here only gives the analytical result of the channel-averaged SINR rather than BER, it is still meaningful in the sense that it can be used to directly compare the performances of different UWB Rake receivers, without resorting to tedious simulation or experimental works. During the final stage of this thesis, we became aware that there is an independent work [22], which derived an exact formula for computing both the channel-averaged SNR and BER. However, their work was based on the assumption that all the MPCs, no matter if they are overlapped in the time domain, can be resolved at the receiver. Generally, this is not true for a realistic Rake receiver, rendering their results less practical. In our work, we have considered the UWB Rake receiver with multipath resolvability approximately equal to the inverse of the system bandwidth, which is a more practical assumption. Consequently, the analytical results we have derived here are more meaningful in this sense.

3.1.1 System Model

We consider a typical indoor multiuser communication scenario and TH-BPPM as the signaling format. The transmissions from different users are assumed to be asynchronous. Each user is assigned a pseudo-random time-hopping sequence to avoid catastrophic collisions with other users. The TH-BPPM signal transmitted by the νth user is [3]

$$s^{(\nu)}(t) = \sum_{j=-\infty}^{+\infty} \sqrt{E_w}\, w_{\mathrm{tr}}(t - jT_f - c_j^{(\nu)} T_c - \delta\, b_{\lfloor j/N_s \rfloor}^{(\nu)}) \tag{3.1}$$

where

- $w_{\mathrm{tr}}(t)$ represents the transmitted pulse with unit energy and a pulse width of T_w
- E_w is the transmitted pulse energy and δ is the timing shift associated with BPPM.
- $b_{\lfloor j/N_s \rfloor}^{(\nu)} \in \{0, 1\}$ is the user-specific data sequence ($\lfloor x \rfloor$ denotes the integer part of x).
- T_f is the frame time and N_s is the number of frames per symbol transmission.
- $c_j^{(\nu)}$ is time-hopping value for the jth frame of the νth user, where $0 \leq c_j^{(\nu)} \leq N_h - 1$
- T_c is the chip duration and $T_c = T_w + \delta$.

To analyze the performance of a practical Rake receiving system, we usually need to make the assumption that the MPCs are isolated and resolvable at the receiver. Based on this assumption, we consider a discrete-time equivalent channel model for (2.4). Specifically, the whole arrival time axis is divided into time bins of $\Delta\tau$ ($\Delta\tau = T_c$), which should be at least equal to the pulse width [5]. In any given time bin, there may be one or more MPCs, or even no MPC arrival at all, depending on the double Poisson arrival process of the MPCs. The channel gain coefficients of all the arrived MPCs within that time bin are added together to yield a combined channel gain coefficient. Based on this model, the νth user's discrete-time channel impulse response can be written as

$$h^{(\nu)}(t) = \sum_{i=1}^{N} A_i^{(\nu)} \delta(t - \tau_i) \tag{3.2}$$

where $\tau_i = (i-1)\Delta\tau$ is the ith time bin and $A_i^{(\nu)}$ represents the sum of the channel gain coefficients of all MPCs arrived in the ith time bin. N is the total number of time bins determined by the delay spread of the underlying channel model. Compared with (2.4), this discrete-time channel model does not account for the pulse distortion due to the partial *pulse overlapping*, which usually happens when the pulse width is large, e.g., 0.7 ns in [14]. However, when considering a pulse width as small as 0.167 ns, the probability of this partial pulse overlapping will be greatly reduced. With this small pulse width, the equivalent sampling frequency for the continuous-time channel impulse response will be about 6 GHz and (3.2) will be a good approximation to (2.4) by preserving most of the channel characteristics.

The signal received by the *desired* first user within one symbol duration can be written as (assuming symbol '0' has been transmitted without loss of generality)

$$\begin{aligned} r(t) = &\sum_{j=0}^{N_s-1} \sqrt{E_w}\, g^{(1)}(t - jT_f - c_j^{(1)} T_c - \delta\, b_{\lfloor j/N_s \rfloor}^{(1)}) \\ &+ \sum_{\nu=2}^{N_u} \sum_{j=-\infty}^{+\infty} \sqrt{E_w}\, g^{(\nu)}(t - jT_f - c_j^{(\nu)} T_c - \delta\, b_{\lfloor j/N_s \rfloor}^{(\nu)} - \tau_0^{(\nu)}) + n(t) \end{aligned} \tag{3.3}$$

where $g^{(\nu)}(t) = w_{\text{rec}}(t) \otimes h^{(\nu)}(t), \nu = 1, 2, \ldots, N_u$ and N_u is the total number of users. $w_{\text{rec}}(t)$ represents the received pulse, which is the time derivative of the transmitted pulse $w_{\text{tr}}(t)$, accounting for the receiver's antenna effect. $h^{(\nu)}(t)$ denotes the discrete-time channel impulse response for the νth user and is considered to be at least time-invariant within one

symbol duration ($\otimes$ denotes the convolution). $\tau_0^{(\nu)}$ represents the νth user's reference delay relative to the first user caused by the asynchronous transmission and we assume $\tau_0^{(1)} = 0$ without loss of generality. $n(t)$ is the AWGN with two-sided power spectral density of $N_o/2$.

3.1.2 Rake Performance Analysis

According to the discrete-time channel model, a tapped-delay-line Rake receiver structure can be adopted to collect the signal energy in each time bin (finger). For the first user, if we assume the perfect timing synchronization has been achieved at each Rake finger, the output of the ith finger can be written as

$$Z_i = \sum_{j=0}^{N_s-1} \int_{\tau_i+jT_f}^{\tau_i+(j+1)T_f} r(t)\, v(t - jT_f - c_j^{(1)}T_c - \tau_i)\, dt \tag{3.4}$$

where $v(t) = w_{\text{rec}}(t) - w_{\text{rec}}(t-\delta)$ is the template signal. Assuming the perfect channel estimation, the decision statistic after the maximal ratio combining (MRC) of the first Q fingers is expressed by

$$Z = \sum_{i=1}^{Q} \sqrt{E_w}\, A_i^{(1)} Z_i \Rightarrow \begin{cases} \text{“0” is transmitted,} & Z \geq 0 \\ \text{“1” is transmitted,} & Z < 0. \end{cases} \tag{3.5}$$

where $A_i^{(1)}$ represents the channel gain coefficient of the ith time bin of the first user and is assumed to be known (perfectly estimated) at the receiver. To avoid the inter-frame interference (IFI), we assume [3]

$$N_h T_c + T_m + T_w + \delta \leq T_f \tag{3.6}$$

where T_m is the channel delay spread, and T_w is the pulse width. Note that (3.6) is different from that in [3], where the authors assumed $N_h T_c + T_m + T_w + \delta \leq T_f/2$. The main purpose is to somehow simplify the analysis. Interested readers are referred to [3] for details.

The channel-averaged SINR is defined as

$$\text{SINR} \triangleq \frac{|\mathbf{E}\{Z\}|^2}{\mathbf{Var}\{\text{Z}\}} \tag{3.7}$$

where $\mathbf{E}\{\cdot\}$ denotes the expectation and $\mathbf{Var}\{\cdot\}$ denotes the variance. According to (3.3), there will be three components in the decision statistic Z, namely the desired signal, the filtered noise and the MAIs from other users. One can easily verify that the filtered noise and

the MAIs from all the interferers are independent zero-mean random variables. Accordingly, the channel-averaged output SINR can be formulated as

$$\mathrm{SINR} = \frac{|\mathbf{E}^{(1)}\{\xi\}|^2}{\mathbf{E}^{(1)}\left\{\sigma_{\mathrm{rec}}^2 + E_w^2 N_s T_f^{-1} \sum_{\nu=2}^{N_u} {G_{\mathrm{eff}}^{(\nu)}}^2\right\}}. \tag{3.8}$$

The quantities ξ, σ_{rec}^2 and ${G_{\mathrm{eff}}^{(\nu)}}^2$, which represent the desired signal, the filtered noise and the MAI from the νth user, respectively, are evaluated as

$$\xi = E_w N_s R(0) \sum_{i=1}^{Q} {A_i^{(1)}}^2 \tag{3.9}$$

$$\sigma_{\mathrm{rec}}^2 = N_o E_w N_s R(0) \sum_{i=1}^{Q} {A_i^{(1)}}^2 \tag{3.10}$$

$${G_{\mathrm{eff}}^{(\nu)}}^2 = \sum_{i=1}^{Q}\sum_{k=1}^{Q}\sum_{n=1}^{N}\sum_{m=1}^{N} A_i^{(1)} A_k^{(1)}\, \mathbf{E}^{(\nu)}\{A_n^{(\nu)} A_m^{(\nu)}\}\, \Psi[(i-k-n+m)\Delta\tau], \tag{3.11}$$

where $\mathbf{E}^{(\nu)}\{\cdot\}$ denotes the expectation with respect to the νth user's channel realizations. $R(\cdot)$ represents the correlation function between the received pulse $w_{\mathrm{rec}}(t)$ and the template signal $v(t)$, defined by $R(\tau) = \int_{-\infty}^{+\infty} w_{\mathrm{rec}}(t) v(t+\tau) d\tau$. $\Psi(\cdot)$ is the autocorrelation function of $R(\tau)$, defined by $\Psi(x) = \int_{-\infty}^{+\infty} R(\tau) R(\tau + x) d\tau$. Note that in deriving (3.8), we have assumed that the TH sequences of different users are independent to each other.

As shown in (3.8), to find the channel-averaged SINR, we need to take another expectation with respect to different channel realizations. Considering the MAI part shown by (3.11), we should first evaluate ${G_{\mathrm{eff}}^{(\nu)}}^2$, which is the expectation with respect to all the interferers' channel realizations. The implicit assumption by doing so is that the MAI is accounted for in terms of the second-order moment due to the *time asynchronism* among different users' transmissions, given the channel gain coefficients of the desired first user that are being perfectly estimated.

For a specific channel realization, we have $A_n^{(\nu)} = \sum_q p_{n,q}^{(\nu)} \beta_{n,q}^{(\nu)}$ and $A_m^{(\nu)} = \sum_u p_{m,u}^{(\nu)} \beta_{m,u}^{(\nu)}$, where $(p_{n,q}^{(\nu)}, p_{m,u}^{(\nu)})$ equiprobably take on the values of ± 1 and $(\beta_{n,q}^{(\nu)}, \beta_{m,u}^{(\nu)})$ represent the qth and the uth MPCs arrived in the nth and the mth time bins, respectively. Note that there are some notational differences between the definitions of the subscripts of $\beta_{n,q}^{(\nu)}$ and that of $\beta_{k,l}$ in (2.4), because the former has taken into account multiple MPCs arrived in one time bin. Due to the independency between different MPCs and the fact that $\mathbf{E}^{(\nu)}\{p_{n,q}^{(\nu)}\} = 0$ and

$\mathbf{E}^{(\nu)}\{p_{n,q}^{(\nu)^2}\} = 1$, we have

$$\mathbf{E}^{(\nu)}\{A_n^{(\nu)}A_m^{(\nu)}\} = \begin{cases} \mathbf{E}^{(\nu)}\{A_n^{(\nu)^2}\} = \sum_q \mathbf{E}^{(\nu)}\{\beta_{n,q}^{(\nu)^2}\}, & n = m \\ 0, & n \neq m. \end{cases} \tag{3.12}$$

Using this result, $G_{\text{eff}}^{(\nu)^2}$ will have nonzero components only when $n = m$. Furthermore, due to the zero-crossing property of $R(\cdot)$ and the limited supporting range of $\Psi(\cdot)$, we have $\Psi(\pm\Delta\tau) \ll \Psi(0)$ and $\Psi[(i-k)\Delta\tau] = 0$ when $|i-k| \geq 2$. Consequently, only the terms corresponding to $i = k$ and $n = m$ will be left, resulting in

$$G_{\text{eff}}^{(\nu)^2} = \Psi(0) \cdot \sum_{i=1}^{Q} A_i^{(1)^2} \cdot \sum_{n=1}^{N} \mathbf{E}^{(\nu)}\{A_n^{(\nu)^2}\}. \tag{3.13}$$

Substituting (3.13) into (3.8), the channel-averaged SINR can be formulated as

$$\text{SINR} = \frac{E_w N_s R^2(0) \sum_{i=1}^{Q} \mathbf{E}^{(1)}\{A_i^{(1)^2}\}}{N_o R(0) + E_w \Psi(0) T_f^{-1} \sum_{\nu=2}^{N_u} \sum_{n=1}^{N} \mathbf{E}^{(\nu)}\{A_n^{(\nu)^2}\}}. \tag{3.14}$$

The computation of (3.14) requires the evaluation of the average path energy. Recalling our discrete-time channel model, there could be one or more MPCs, or even no MPC arrival at all, in any given time bin. In the following, when we mention a *cluster arrival* in any given time bin, we refer to the arrival of the first ray within this cluster. Accordingly, a *ray arrival* is always referring to the arrival of a ray other than the first one within each cluster.

With the very small $\Delta\tau$ in our assumption, it is well known that Poisson arrival process can be approximated by Binomial distribution. Specifically, there could be one or no cluster arrival in $\Delta\tau$ with the probabilities given by $P_c \triangleq \Lambda\Delta\tau$ and $1 - P_c$, respectively. In addition, given a cluster arrival in a certain time bin, there could be one or no ray arrival in any of its following time bins with the probabilities given by $P_r \triangleq \lambda\Delta\tau$ and $1 - P_r$, respectively (recall that $1/\Lambda$ and $1/\lambda$ are defined as the cluster and the ray arrival rates, respectively). Because the time bin under consideration is very small, the probability that there are more than one cluster arrival in any time bin is negligible. Similarly, within the same cluster, the probability that there are more than one ray arrival in any time bin is also negligible. Based on this assumption, there are only a *finite number* of arrival patterns in each time bin and the average path energy, as shown later, can be evaluated in a unified way no matter which channel model has been chosen, i.e., line-of-sight (LOS) or non-line-of-sight (NLOS).

In the evaluation of the *average path energy*, we find the following lemma useful.

Lemma 1: Define $P_q^{(n)}$ as the probability that the qth time bin has an MPC contribution to the nth ($n \geq 2$) time bin. It can be calculated in three cases:

$$P_q^{(n)} = \begin{cases} P_r, & q = 1 \\ P_c \cdot P_r, & 2 \leq q \leq n-1 \\ P_c, & q = n \end{cases} \tag{3.15}$$

Proof of lemma 1: see Appendix A.1.

It is very interesting to observe that, the probability that the qth ($q = 1, 2, \ldots, n-1$) time bin has a *ray* contribution to the nth time bin can be simply calculated as the joint probability that a cluster arrives at the qth time bin and this cluster results in a ray at the nth time bin.

Using lemma 1 and enumerating all possible arrival patterns in the nth time bin, the average path energy can be evaluated in Appendix A.2 as

$$\mathbf{E}^{(\nu)}\{A_n^{(\nu)^2}\} = \begin{cases} \Omega_0, & \text{for } n = 1 \\ \Omega_0 P_c \exp\left[-\dfrac{(n-1)\Delta\tau}{\Gamma}\right] + \Omega_0 P_r \exp\left[-\dfrac{(n-1)\Delta\tau}{\gamma}\right] & \\ + \Omega_0 P_c P_r \dfrac{\rho^2(1-\rho^{n-2})}{1-\rho} \exp\left[-\dfrac{n\Delta\tau}{\gamma} + \dfrac{\Delta\tau}{\Gamma}\right], & \text{for } n \geq 2 \end{cases} \tag{3.16}$$

where $\rho = \exp\left(\frac{\Delta\tau}{\gamma} - \frac{\Delta\tau}{\Gamma}\right)$. Note that the user-specific superscript ν has been omitted in the final expression for notational simplicity, implying that all users experience the same type of indoor wireless channel without loss of generality. It should be pointed out that, by defining $\bar{E}_c \triangleq \sum_{n=1}^{N} \mathbf{E}^{(\nu)}\{A_n^{(\nu)^2}\}$, we can now theoretically set

$$\Omega_0 = \frac{1}{\bar{E}_0} \triangleq \frac{1}{\bar{E}_c|_{\Omega_0=1}} \tag{3.17}$$

so as to make $\bar{E}_c = 1$ (normalized), instead of normalizing the total channel energy, defined as $\mathbf{E}\{\sum_{l=1}^{L}\sum_{k=1}^{K}\alpha_{k,l}^2\}$ in [34], for each realization. Although the later was defined as the total channel energy, our definition is more practical in the sense that the receiver can not distinguish the MPCs arrived in the same time bin, thus can not collect the energy from these MPCs separately.

By selecting $\Omega_0 = \bar{E}_0^{-1}$ for each user and substituting (3.16) into (3.14), the channel-averaged SINR can be derived as

$$\text{SINR} = \frac{E_w N_s R^2(0)\bar{E}_0^{-1}}{N_o R(0) + E_w \Psi(0) T_f^{-1}(N_u - 1)} \left\{ 1 + P_c \frac{\exp\left(-\frac{\Delta\tau}{\Gamma}\right) - \exp\left(-\frac{Q\Delta\tau}{\Gamma}\right)}{1 - \exp\left(-\frac{\Delta\tau}{\Gamma}\right)} \right.$$

$$+ P_r \frac{\exp\left(-\frac{\Delta\tau}{\gamma}\right) - \exp\left(-\frac{Q\Delta\tau}{\gamma}\right)}{1 - \exp\left(-\frac{\Delta\tau}{\gamma}\right)} + P_c P_r \frac{\rho^2 \exp\left(\frac{\Delta\tau}{\Gamma}\right)}{1-\rho} \left[\frac{\exp\left(-\frac{2\Delta\tau}{\gamma}\right) - \exp\left(-\frac{(Q+1)\Delta\tau}{\gamma}\right)}{1 - \exp\left(-\frac{\Delta\tau}{\gamma}\right)} \right.$$

$$\left. \left. - \frac{\exp\left(-\frac{2\Delta\tau}{\gamma}\right) - \rho^{Q-1} \exp\left(-\frac{(Q+1)\Delta\tau}{\gamma}\right)}{1 - \exp\left(-\frac{\Delta\tau}{\Gamma}\right)} \right] \right\}. \tag{3.18}$$

Notable about (3.18) is that it has incorporated all the channel model parameters, thus is easy to evaluate without requiring any further simulation works. Meanwhile, it is a natural attempt to derive a closed-form expression for the *channel-averaged* BER based on our discrete-time channel model. Unfortunately, to the best of the authors' efforts, we found that without much changing the essence of IEEE 802.15.3a channel model, the derivation of a closed-form BER expression is unwieldy. The main difficulty lies in the fact that, as far as the higher-order moments are concerned rather than the first and the second-order moments considered here, the statistical independency among different time bins is no longer held due to the possible overlapping between the adjacent clusters, which has led to an extremely hard task to derive an exact probability density function (pdf) for the combined channel gain coefficient of each time bin. Despite of this, (3.18) is still valuable in the sense that it provides a closed-form expression for the channel-averaged SINR which can be directly used to predict UWB Rake system performance in different types of indoor wireless channel models.

3.2 UWB-TR system

In this section, we apply the theoretical framwork we just developed to the UWB-TR system to evaluate its channel-averaged SINR. Specifically, we consider UWB-TR system using frame-rate correlation as most existing works. Another application of the theoretical framework developed here is to determine the optimum integration interval for the UWB-TR system so as to maximize its average output SINR. This issue has been addressed by several previous papers [12, 14]. However, all these works only considered optimizing the integration interval in single-user UWB-TR system. Besides, the optimum integration interval is found via simulation. In this section, we directly apply our theoretical framework, which will enable us to optimize the integration interval analytically, even in a multiuser scenario.

3.2.1 System Model

The transmitted signal from the νth user using binary antipodal modulation can be written as [14]

$$s^{(\nu)}(t) = \sum_{j=-\infty}^{+\infty} \sqrt{E_w}\, d_j^{(\nu)} \Big[w_{\mathrm{tr}}(t - jT_f - c_j^{(\nu)} T_c - \tau_0^{(\nu)}) + b_{\lfloor j/N_s \rfloor}^{(\nu)} w_{\mathrm{tr}}(t - jT_f - c_j^{(\nu)} T_c - T_d^{(\nu)} - \tau_0^{(\nu)}) \Big] \tag{3.19}$$

where all the parameters are same as in Section 3.1 except

- $T_d^{(\nu)}$ is the user-specific delay between the reference and the data pulses.
- $d_j^{(\nu)}$ is a pseudo-random $\{\pm 1\}$ sequence to randomize the polarities of the pulses.
- T_c is the chip duration and $T_c = T_w$.

In (3.19), two pulses are transmitted in each frame, corresponding to the reference and data pulses, respectively. In order to avoid the inter-pulse interference (IPI) between the reference and data pulses after transmitting through the multipath channel, $T_d^{(\nu)}$ is assumed to be larger than the channel delay spread T_m. Note that $T_d^{(\nu)}$ is set to different values for different users, the reason for which will be explained later. In addition, the frame time T_f is assumed to be larger than $N_h^{(\nu)} T_c + T_m + T_w + T_d^{(\nu)}$ to ensure that there is no inter-frame interference (IFI). Note that the maximum time-hopping shift $N_h^{(\nu)} T_c$ should be set according to $T_d^{(\nu)}$ in order to keep the frame time T_f fixed for all users [14].

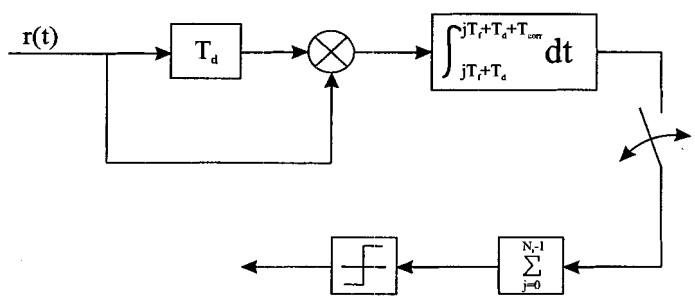

Figure 3.1: TR receiver.

A UWB-TR receiver structure using frame-rate correlator is shown in Fig. 3.1. Note that in Fig. 3.1, the integration-and-dump operation is on the frame rate and the frame

outputs are finally summed up before making the decision. In a multiuser scenario, to detect the νth user's transmitted symbols, the decision statistic can be expressed as

$$Z^{(\nu)} = \sum_{j=0}^{N_s-1} \int_{jT_f+c_j^{(\nu)}T_c+T_d^{(\nu)}}^{jT_f+c_j^{(\nu)}T_c+T_d^{(\nu)}+T_{\text{corr}}} r(t)\, r(t-T_d^{(\nu)})\, dt \tag{3.20}$$

where T_{corr} is assumed to be an integer multiple of the chip duration, denoted by QT_c and time asynchronism $\tau_0^{(\nu)}$ is assumed to be zero for the reception of the νth user's signal, without loss of generality.

3.2.2 Single-user UWB-TR system

In a single-user UWB-TR system, the received signal in one symbol duration is written as

$$r(t) = \sum_{j=0}^{N_s-1} \sqrt{E_w}\; d_j\Big[g(t-jT_f-c_jT_c) + \; b_{\lfloor j/N_s \rfloor} g(t-jT_f-T_d-c_jT_c)\Big] + n(t) \tag{3.21}$$

where $g(t)$ has similar definition as in (3.3). Note that we have omitted the user-specific superscript ν and asynchronous transmission delays. Using the frame-rate correlation receiver mentioned above, the channel-averaged output SNR can be derived in Appendix A.3 as a function of the integration interval via Q, denoted by

$$\text{SNR}(Q) = \frac{N_s E_w^2 \left[G^{(1)}(Q)\right]^2}{N_o E_w G^{(1)}(Q) + N_o^2\, WQT_c/2} \tag{3.22}$$

where $G^{(1)}(Q) \triangleq \sum_{i=1}^{Q} \mathbf{E}^{(1)}\{{A_i^{(1)}}^2\}$ can be evaluated using (3.16), and W represents one-sided receiver bandwidth. As shown in Appendix A.3, the two terms in the denominator represent noise-times-signal and noise-times-noise terms, respectively. By substituting (3.16) into (3.22), we can theoretically choose the optimum integration interval to maximize the average output SNR, given by

$$Q^{\text{opt}} = \underset{Q}{\text{argmax}} \Big\{\text{SNR}(Q)\Big\}, \tag{3.23}$$

which is a function of the channel model parameters, transmitted pulse energy, noise power spectral density, the receiver bandwidth and the chip duration (or the pulse width).

An interesting point here is, depending upon the input SNR, we will have different optimum integration intervals. Intuitively, as the input SNR increases, the optimum integration interval will increase as well. The extreme case is, when the input SNR is very large, the

noise-times-noise term in (3.22) can be ignored compared to the noise-times-signal term and the optimum integration interval will span all the MPCs. Similarly, the optimum integration interval will decrease when the input SNR gets lower. The extreme case is, when the input SNR is very low, the noise-times-signal term can be ignored and the optimum integration interval becomes a constant which no longer depends on the input SNR.

3.2.3 Multiuser UWB-TR system

In the multiuser scenario, the signal within one symbol duration received by the desired first user can be written as

$$r(t) = \sum_{j=0}^{N_s-1} \sqrt{E_w} d_j^{(1)} \left[g^{(1)}(t - jT_f - c_j^{(1)} T_c) + b_{\lfloor j/N_s \rfloor}^{(1)} g^{(1)}(t - jT_f - c_j^{(1)} T_c - T_d^{(1)}) \right] + n(t)$$

$$+ \sum_{\nu=2}^{N_u} \sum_{j=-\infty}^{+\infty} \sqrt{E_w} d_j^{(\nu)} \left[g^{(\nu)}(t - jT_f - c_j^{(\nu)} T_c - \tau_0^{(\nu)}) + b_{\lfloor j/N_s \rfloor}^{(\nu)} g^{(\nu)}(t - jT_f - c_j^{(\nu)} T_c - T_d^{(\nu)} - \tau_0^{(\nu)}) \right] \tag{3.24}$$

Similar to the single-user case, the interference can be classified into three uncorrelated terms, such as MAI-times-signal, MAI-times-noise and MAI-times-MAI.

As mentioned earlier, $T_d^{(\nu)}$ and $N_h^{(\nu)}$ are intentionally set to different values for different users. For instance, we may choose

$$\begin{aligned} T_d^{(\nu)} &= T_m + \frac{(\nu - 1)T_c}{2} \\ N_h^{(\nu)} &= N_h^{(N_u)} + \left\lfloor \frac{N_u - \nu}{2} \right\rfloor \end{aligned} \tag{3.25}$$

The main purpose for choosing different $T_d^{(\nu)}$ for different users is to intentionally misalign the interferer's reference with its associated data signal, so as to reduce the MAI-times-MAI term. As shown in Appendix A.3, the MAI-times-MAI can be further classified as two components. One is the total interference resulting from the correlation of the signals from the *same* interferer, termed it as self-MAI-times-MAI; the other one is the total inteference resulting from the correlation of the signals from *different* interferers, termed it as cross-MAI-times-MAI. With the above signaling format, the contribution from self-MAI-times-MAI will be relatively small compared to cross-MAI-times-MAI, especially when the number of users is large. As a result, we ignore the self-MAI-times-MAI term in the analysis for the average output SINR and the accuracy of this approximation will be verified by simulations later.

Based on that, the channel-averaged output SINR in the multiuser scenario is evaluated in Appendix A.3:

$$\begin{aligned}\mathrm{SINR}(Q) &= N_s E_w^2 \left[G^{(1)}(Q)\right]^2 \Bigg\{ N_o E_w G^{(1)}(Q) + N_o^2 W Q T_c/2 \\ &+ \frac{4(N_u-1)}{T_f} E_w^2 \Psi(0) G^{(1)}(Q) + \frac{2(N_u-1)}{T_f} E_w N_o Q T_c + \frac{4(N_u-1)(N_u-2)}{{T_f}^2} \\ &\times \left[\int_0^{T_c} \int_{-y}^{T_c} R_w^2(x) dx dy + \int_0^{T_c} \int_{-T_c}^{T_c-y} R_w^2(x)\, dx\, dy + \Psi(0)(Q-2)T_c \right] \Bigg\}^{-1} \end{aligned} \tag{3.26}$$

where $R_w(\cdot)$ is the autocorrelation function of the received pulse, defined as $R_w(\tau) = \int_{-\infty}^{+\infty} w_{\mathrm{rec}}(t) w_{\mathrm{rec}}(t+\tau) dt$. Again, the optimum integration interval can be determined by (3.23) except substituting (3.26) as the objective function to be maximized. It is obvious that, as far as the MAI is included, the optimum integration interval will be different from that for the single-user UWB-TR system.

3.3 Performance Results

In this section, we present some performance results for the analyses in Sections 3.1 and 3.2. We choose $N = 200$ for CM1, CM2 and $N = 400$ for CM3, CM4, because the channel models CM1, CM2 and CM3, CM4 have similar channel delay spreads, respectively. Note that $\Delta\tau$ is chosen to be 0.167 ns, which is equal to the chip duration T_c. Accordingly, $\bar{E}_0$ in (3.17) is calculated for the channel models CM1, CM2, CM3 and CM4, as shown in Table 3.1. In Table 3.1, the total channel energy was also calculated using sufficiently large N, i.e., $N = \lfloor 10(\Gamma+\gamma)/\Delta\tau \rfloor$ as suggested in [34]. It can be seen that we have captured most of the signal energy when $N = 200$ for CM1, CM2 and $N = 400$ for CM3, CM4.

Table 3.1: Average total channel energy for indoor UWB channel models.

$\bar{E}_0$	CM1	CM2	$\bar{E}_0$	CM3	CM4
$N = 200$	13.3837	13.4105	$N = 400$	33.2722	62.5121
$N = \lfloor \frac{10(\Gamma+\gamma)}{\Delta\tau} \rfloor$	13.4297	13.6438	$N = \lfloor \frac{10(\Gamma+\gamma)}{\Delta\tau} \rfloor$	33.5808	67.5412

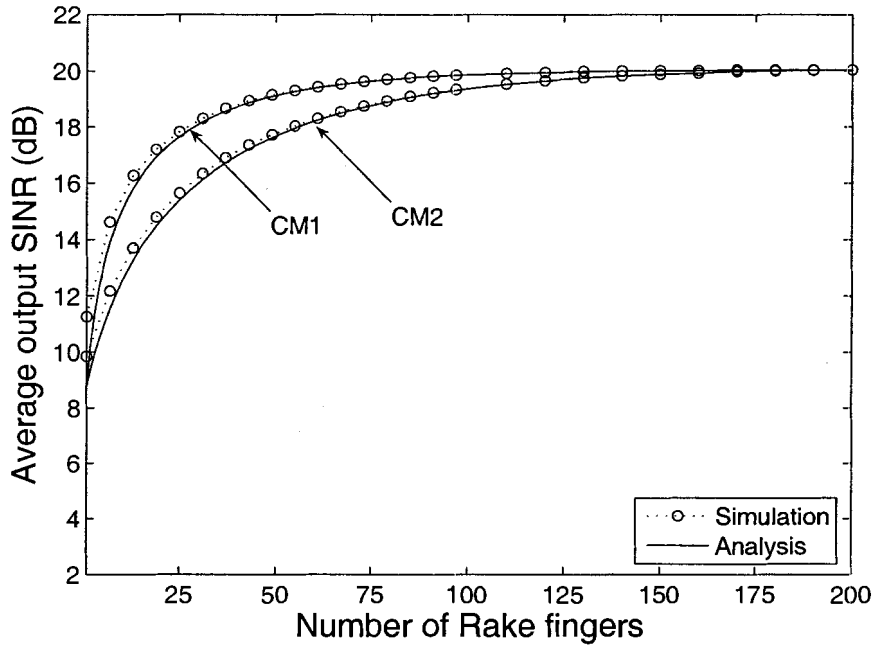

Figure 3.2: Average output SINR versus the number of Rake fingers Q for CM1, CM2 when $E_b/N_o = 20$dB.

In our simulation for UWB Rake receiving system, we first consider an indoor multiuser scenario where $N_u = 20$ users transmit TH-BPPM signals and a UWB Rake receiver tries to detect the signal coming from the *desired* first user. All 20 users are assumed to experience the same type of channel model. The ideally received pulse is assumed to be the second-order derivative of the Gaussian pulse with a pulse width slightly less than $\Delta\tau$ so as to accommodate the timing shift δ associated with BPPM. The transmitted pulse energy is normalized to $E_w = 1$. The maximum time hopping value N_h is chosen to be 64. The frame time T_f is 1000 chips, which is equal to 167 ns and the number of frames per symbol transmission is chosen as $N_s = 1$ without lost of generality.

Fig. 3.2 shows the average output SINR versus the number of Rake fingers for the channel models CM1 and CM2, when $E_b/N_o \triangleq N_s E_w/N_o = 20\,\text{dB}$. It can be easily observed that, when the number of Rake fingers Q is greater than 50 for CM1 and 75 for CM2, there will be little increment for the collected signal energy. It is obvious that our analysis well

matches with the simulation results. The little discrepancies occurring for the small number of Rake fingers are mainly due to that the 0.167 ns time bin is not small enough to well approximate the Poisson process by the Binomial distribution. Fig. 3.3 shows the average output SINR versus the number of Rake fingers for the channel models CM3 and CM4, when $E_b/N_o = 20\,\text{dB}$. Similarly, when the number of Rake fingers Q is greater than 100 for CM3 and 150 for CM4, increasing Q will not much increase the collected signal energy. By observing Figs. 3.2 and 3.3, a direct conclusion we can draw is, to collect enough signal energy, a UWB Rake receiver has to implement a large number (tens or even hundreds) of Rake fingers, which poses great challenges for the design of a low-cost and low-complexity UWB Rake receiver.

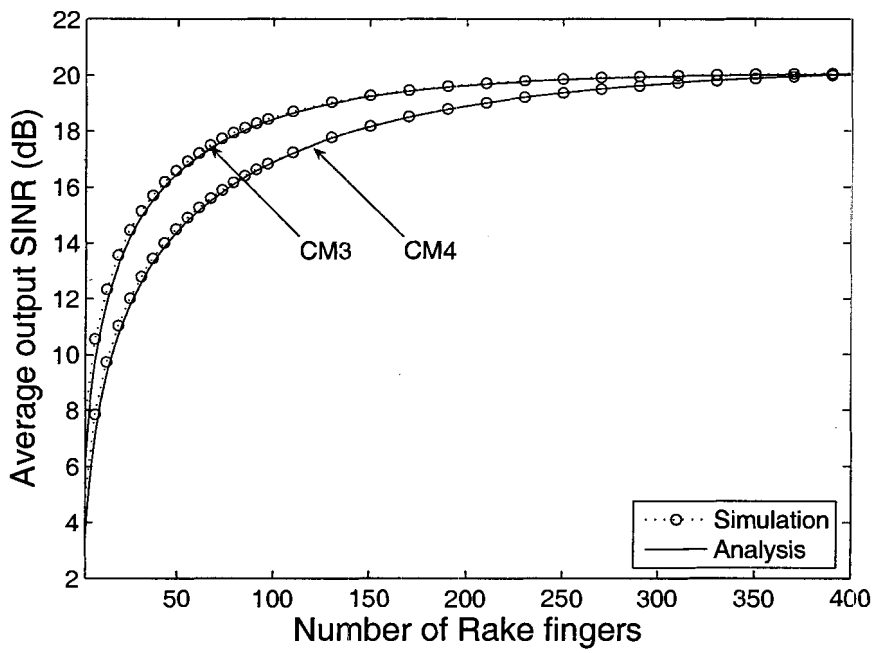

Figure 3.3: Average output SINR versus the number of Rake fingers Q for CM3, CM4 when $E_b/N_o = 20\text{dB}$.

In our simulation for UWB-TR system, the chip duration T_c is equal to the pulse width T_w, since we are using BPAM in stead of BPPM. The frame time T_f is again chosen to be 1000 chips, equivalent to 167 ns, in order to make a fair comparison between the UWB Rake

and TR systems. All other simulation parameters remain same as in UWB Rake system.

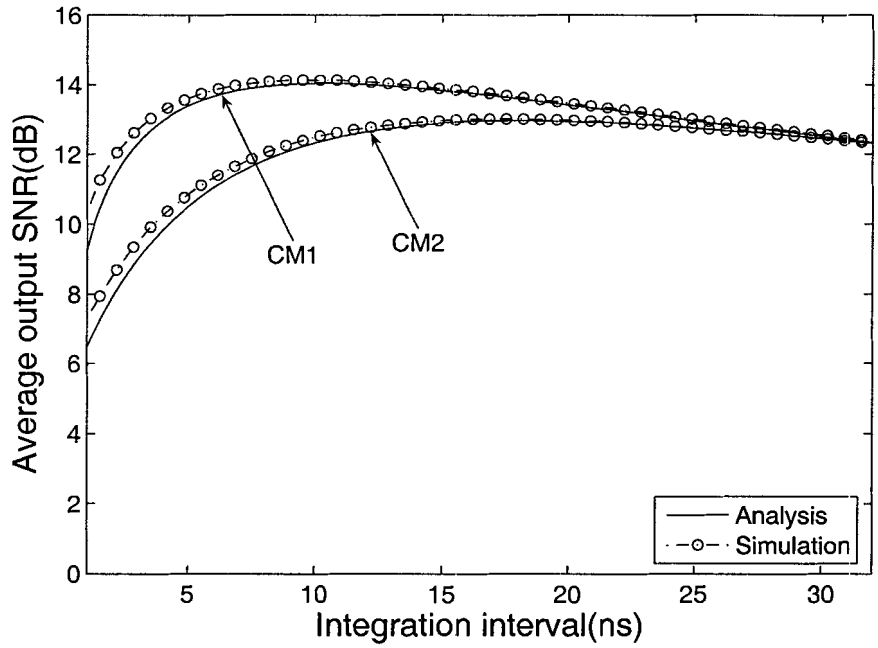

Figure 3.4: Average output SNR versus the integration interval for CM1, CM2 when $E_b/N_o = 20$dB.

Fig. 3.4 shows the average output SNR versus the integration interval for a single-user UWB-TR system for CM1 and CM2. Clearly, in UWB-TR system, increasing the integration interval does not always guarantee the increased output SNR. At certain point, the output SNR will decrease as the integration interval increases. The reason for this is obvious. According to the power delay profile (PDP), the MPCs arrived with larger delays usually have smaller signal energy, or equivalently smaller SNR. As a result, integrating over these MPCs will accumulate more noise energy than the desired signal energy, eventually leading to decreased SNR. Another observation from Fig. 3.4 is the maximum average output SNRs in CM1 and CM2 are around 14 dB and 12 dB, achieved with the integration intervals of 9.5 ns and 17.5 ns, respectively. By comparing Fig. 3.4 with Fig. 3.2, we find that UWB-TR system suffers a significant SNR loss (almost 6 dB) compared to UWB Rake receiver, although Fig. 3.2 has included the MAI. Similar results can also be found for CM3

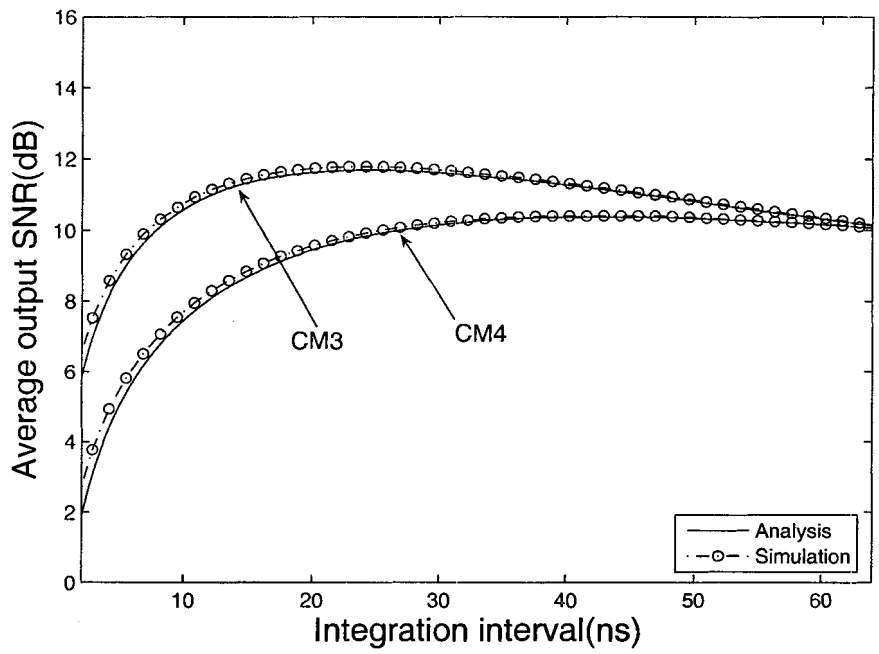

Figure 3.5: Average output SNR versus the integration interval for CM3, CM4 when $E_b/N_o = 20$dB.

and CM4, as shown in Fig. 3.5, in which the maximum output SNRs are achieved with the integration intervals of 23.0 ns and 42.9 ns for CM3 to CM4, respectively. However, this comparison is not fair because UWB Rake receiver has to achieve perfect channel estimation and timing synchronization in order to collect the signal energy coherently. Especially, with the large number of Rake fingers we mentioned, it is not feasible to implement such a Rake receiver which can achieve perfect channel estimation. UWB-TR system, on the other hand, greatly reduces the receiver complexity by eliminating the need to estimate the channel at the expense of some performance degradations. Consequently, a good trade-off between the system performance and the complexity has become the driving force behind most of the researches on UWB-TR systems.

In Figs. 3.4 and 3.5, we identify that there exists an optimal integration interval which maximizes the average output SNR. As explained in Section 3.2, this optimal integration varies according to the input SNR. Fig. 3.6 examines this behavior by plotting the optimum

integration interval versus the input SNR for CM1 to CM4. It is observed that when the input SNR increases, the optimum integration interval also increases as expected. When the input SNR is very large, the optimum integration interval will be equal to the channel delay spread. We also find that, when the input SNR is very small, there exist lower bounds on the optimum integration interval for all the channel models, which are found to be 4.7 ns, 13.0 ns, 18.0 ns, and 35.7 ns for CM1 to CM4, respectively. This is an important system design parameter in the sense that, in order to ensure a maximum average output SNR, the integration interval should be at least equal to this value. It should also be pointed out that the integration interval determined by maximizing the average output SNR may not be optimum in terms of minimizing the average BER. To make a comparison, Fig. 3.6 also included the integration intervals corresponding to the minimum average BER for each input SNR. It is obvious that the two criterions yield similar results for low and medium SNR regions, while exhibiting obvious differences for high SNR region.

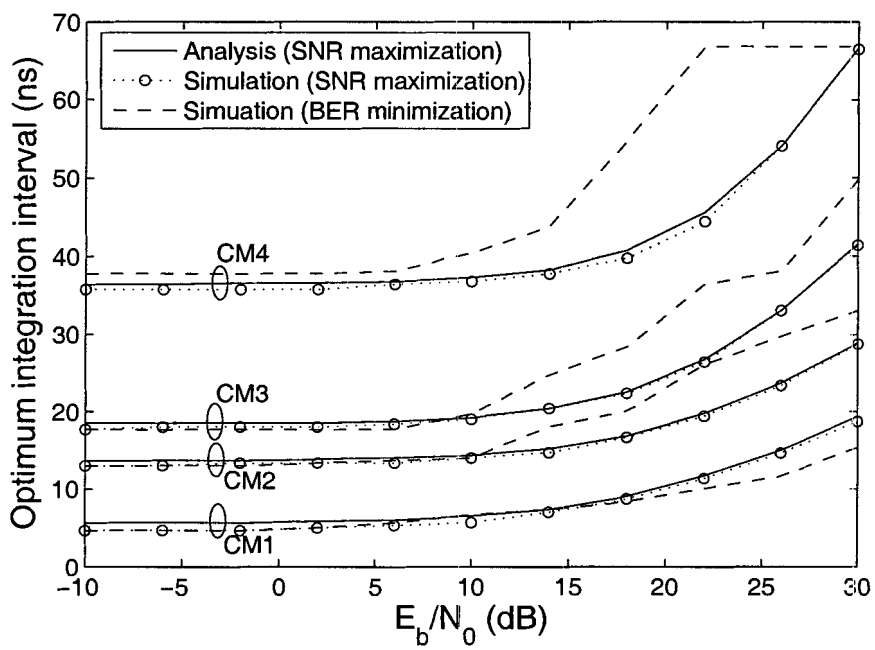

Figure 3.6: Optimum integration interval versus E_b/N_o for 4 different types of channel models CM1 to CM4.

Fig. 3.7 show the average BER performance for a single-user UWB-TR system for CM2 and CM4, respectively. Here, we compare the performance of the scheme that *adaptively* chooses the optimum integration interval depending on the input SNR, with the one using the lower bound for all input SNR values. As a benchmark, we also include the scheme minimizing the average BER. It is easy to find that the adaptive scheme achieves almost the same performance as the one minimizing average BER. Moreover, it outperforms the one using the lower bound as the input SNR increases.

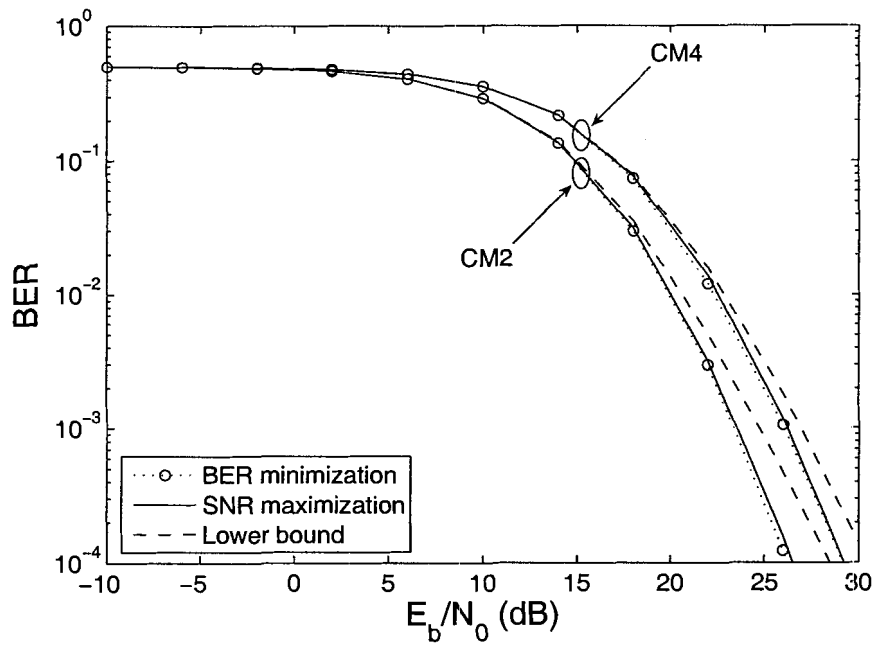

Figure 3.7: BER performance versus E_b/N_o with adaptively selected integration intervals for CM2 and CM4.

In the next two figures, we present some results for the multiuser UWB-TR system. Specifically, we focus on how the optimum integration interval will change when the MAI is taken into account. We will demonstrate that, by using (3.26), one can easily determine an appropriate integration interval in a multiuser UWB-TR system. First, Fig. 3.8 provides the verification of the approximation made in deriving (3.26), i.e., ignoring the self-MAI-times-MAI term, when analyzing the channel-averaged output SINR for the multiuser UWB-TR

system. As an example, the average output SINR for CM1 is plotted for different input SNR values. Note that we have used the integration interval equal to channel delay spread T_m, which is shown to correspond to the worst case for our approximation. In other words, the approximation becomes more accurate as the integration interval decreases. As we can see, the approximation approaches the simulation results as the number of users increases and the discrepancies become negligible as the input SNR goes to as low as 10 dB. Especially, for the low and medium SNRs, our approximation matches quite well with the simulation results.

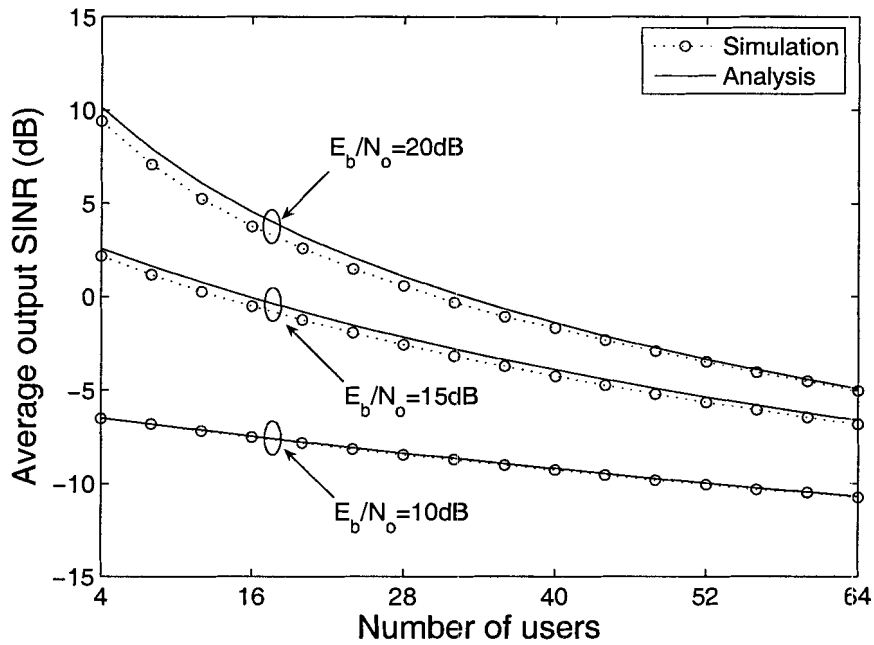

Figure 3.8: Average output SINR versus number of users for varying E_b/N_o for CM1.

Fig. 3.9 shows the theoretical optimum integration interval for the multiuser UWB-TR system for CM1 and CM3, using (3.26) as the target function to be maximized with respect to Q. It is found that, as far as the MAI is concerned, the optimum integration interval will decrease compared to a single-user UWB-TR system. Especially, when the number of users is large, the optimum integration interval approaches the lower bound that has been observed in the single-user system for very low input SNR. This result, combined

with Fig. 3.7, suggests that in the dense multiuser UWB-TR system, a good choice for the integration interval is to simply use the lower bound, which somehow reduces receiver complexity (shorter and fixed integration time) without causing too much performance loss.

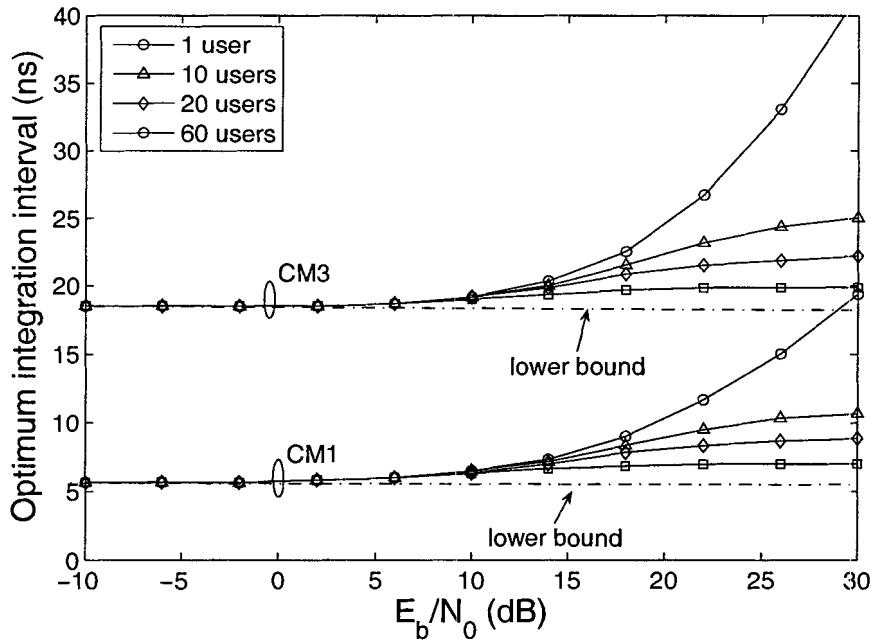

Figure 3.9: Optimum integration interval versus E_b/N_o for CM1 and CM3 under the multiuser scenario.

3.4 Conclusion

In this chapter, we have derived a theoretical closed-form expression for the channel-averaged output SINR under the IEEE 802.15.3a channel model, assuming the UWB Rake receiver in a multiuser communication scenario. The theoretical framework developed here can be directly used to evaluate the channel-averaged output SINR to compare the performances of the UWB Rake receiving system under different types of indoor wireless channel models. This framework is also applicable to UWB-TR systems and enables us to theoretically determine the optimum integration interval that yields the maximum average output SNR.

We investigated the BER performance using the optimum integration interval and observed that using the lower bound as the integration interval for all input SNRs causes some performance loss. We extended the analysis to the multiuser UWB-TR system and demonstrated that the optimum integration interval is different from that in a single-user system. We also found that, in the multiuser scenario, using the lower bound as the integration interval is a good choice, especially in the dense multiuser system.

It is also obvious that UWB-TR system suffers a significant performance loss, compared to the ideal Rake receiving scheme. Consequently, in Chapter 3, we will focus on how to improve the performance of UWB-TR system.

Chapter 4

M-ary Orthogonal Coded/Balanced TR UWB system

In this chapter, we propose a novel UWB-TR system, namely M-ary orthogonal coded/ Balanced TR scheme [20][1], for increasing the information rate and improving the detection performance. The idea was developed based on [16], in which the authors proposed a hybrid matched filter correlator UWB-TR receiver. As can be seen from [16], the usage of their proposed TR receiver leads to better BER performance than the standard TR system using frame-rate correlator which has been discussed in Chapter 3. Consequently, in this chapter, all the performance comparisons will be carried out between our proposed system and the TR system using hybrid matched filter correlator receiver. We will demonstrate that our proposed system has better BER performance, even when operating at higher information rates, than their TR system. To clearly characterize the proposed system, we will first describe this hybrid matched filter correlator TR system in Section 4.1 and then elaborate on the proposed system in Section 4.2. Finally, we present detailed performance analysis as well as simulation results.

[1]© 2006 IEEE. Reprinted, with permission, from *Proc. IEEE ICC'06*, Istanbul, Turkey, June 2006.
This material is posted here with permission of the IEEE. Such permission of the IEEE does not in any way imply IEEE endorsement of any of Simon Fraser University (SFU)'s [Library & Archives Canada's] products or services. Internal or personal use of this material is permitted. However, permission to reprint/republish this material for advertising or promotional purposes or for creating new collective works for resale or redistribution must be obtained from the IEEE by writing to pubs-permissions@ieee.org. By choosing to view this document, you agree to all provisions of the copyright laws protecting it.

4.1 Hybrid Matched Filter Correlator UWB-TR receiver

The UWB-TR system described in Chapter 3 uses the frame rate cross-correlator and has been shown to have some performance loss compared to a coherent Rake receiver. In [16] and [17], the authors proposed and analyzed the performance of a hybrid matched filter correlator UWB-TR system. The receiver structure is shown in Fig. 4.1. Specifically, the received signal first passes through a matched filter whose impulse response is matched to the template signals for the entire symbol duration. Then, the filtered output is fed to a delay-and-correlate unit to collect the signal energy for detecting the transmitted data bit. By using a symbol-rate matched filter before cross-correlation, the receiver not only achieves the noise-averaging, but also allows for the ensuing digital processing to operate at the symbol rate rather than the frame rate, thus reduce the circuit complexity and the power consumptions.

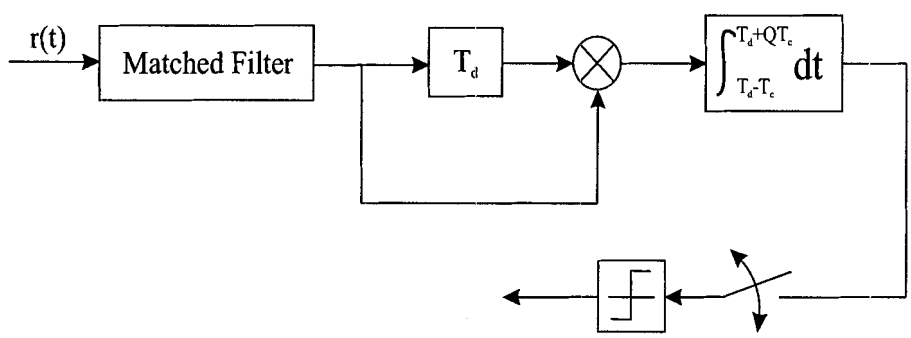

Figure 4.1: Hybrid matched filter correlation TR receiver structure.

As in other UWB-TR systems, the distance between the reference and the data pulses still has to be larger than the channel delay spread to ensure there is no inter-pulse interference (IPI). This will significantly limit the system's achievable information rate. In the rest of this chapter, we will simply refer to this TR system as the *conventional* TR system.

4.2 M-ary Orthogonal Coded/Balanced UWB-TR system

In this section, by describing the system structure of our proposed UWB-TR system, we demonstrate how it suppresses the IPI in a simple but effective way. To deal with the IPI,

there is another method, called maximum likelihood template estimator, proposed by [19]. However, the complexity associated with maximum likelihood template estimation is high, rendering their approach less practical. In addition, during the final stage of this thesis work, we were informed that there was another approach called dual pulse transmission proposed by [23], which is also able to suppress the IPI. However, as shown later, it can be viewed as one special case of our scheme. Our system acts as a generalization to their approach and further introduces a new M-ary orthogonal coded signaling to avoid the inter-frame interference that is detrimental to achieving high-rate transmission in dense multipath, especially for TR systems.

4.2.1 Transmitter

The block diagram of the transmitter is shown in Fig. 4.2. The transmitter includes two parts: an encoder and a standard TR modulator. For simplicity, no time-hopping sequence has been considered. However, it can be included without any difficulty. In Fig. 4.2, $\mathbf{B}_i$ is the ith symbol including $1 + \log_2 M$ data bits, denoted by $\mathbf{B}_i = (b_i\, b_{i+1} \ldots b_{i+\log_2 M})$ where $b_{i+n} \in \{0, 1\}$ for $n = 0, 1, \ldots, \log_2 M$. At the encoder, the $\log_2 M$ bits, denoted by $\mathbf{I}_i = (b_{i+1}\, b_{i+2} \ldots b_{i+\log_2 M})$, are used to select one of the M-ary orthogonal codes. The index of the selected code, denoted by m, is determined by

$$(m)_2 = \left(b_{i+1}\, b_{i+2} \ldots b_{i+\log_2 M}\right) \tag{4.1}$$

where $(\cdot)_x$ denotes base x. The selected orthogonal code is an N_s-element vector, defined by $\mathbf{V}^m = (v_0^m\, v_1^m \ldots v_{N_s-1}^m)$ where $v_n^m \in \{+1, -1\}$ for $n = 0, 1, \ldots, N_s - 1$. The signaling format and the orthogonal codes are designed to meet the following two criterions:

1) the number of frames per symbol, N_s, should be an even number and the numbers of +1 and -1 in each code vector should be equal, i.e., $N_s/2$ elements are +1 and $N_s/2$ are -1;

2) the M-ary codes are orthogonal to each other, i.e., $\sum_{n=0}^{N_s-1} v_n^m\, v_n^k = 0$ for $m \neq k$ where $m, k \in \{0, 1, \ldots, M-1\}$

Note that if $M = 1$, there is no code selection. In this case, we use a fixed code which meets the first criterion for all the symbol transmissions. The specific reasons for these two design criterions will be explained later when we describe the proposed receiver structure. By multiplying $\mathbf{V}^m$ with $\tilde{b}_i$, which equals to +1 if $b_i = 1$ and -1 if $b_i = 0$, we will get an N_s-element vector $\tilde{\mathbf{V}}_i = (\tilde{v}_{i,0}\, \tilde{v}_{i,1} \ldots \tilde{v}_{i,N_s-1})$, where $\tilde{v}_{i,n} = \tilde{b}_i\, v_n^m$ for $n = 0, 1, \ldots, N_s - 1$. $\tilde{\mathbf{V}}_i$

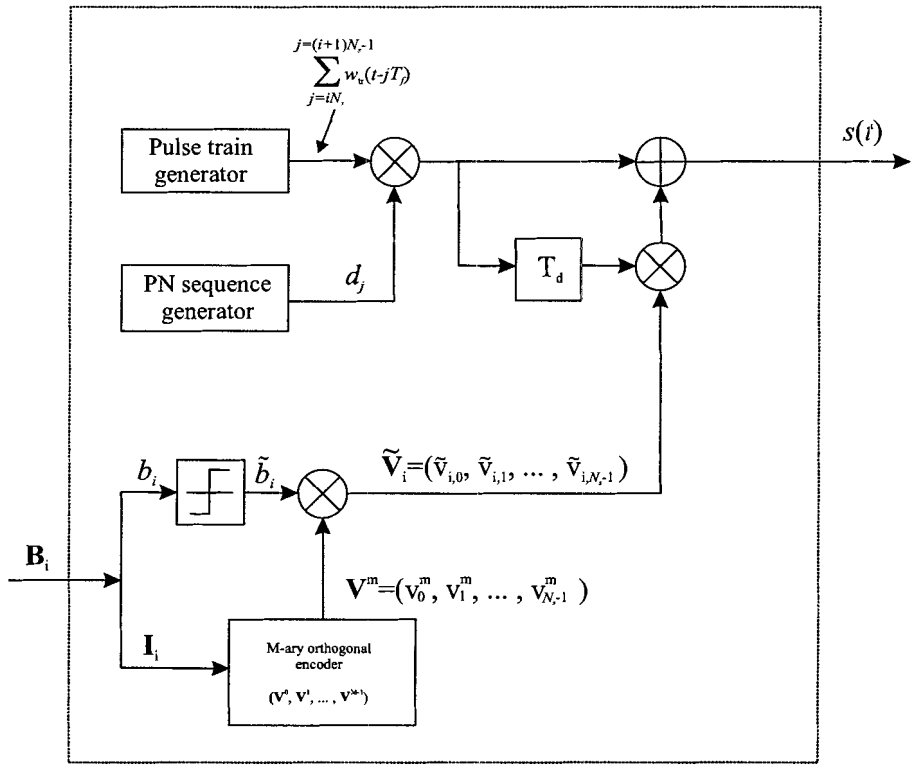

Figure 4.2: M-ary orthogonal coded/Balanced TR system: the transmitter.

is then fed to a standard TR transmitter. The transmitter generates N_s pulse pairs for each symbol transmission. The N_s elements of $\tilde{\mathbf{V}}_i$ determine the polarities of the data pulses in these N_s pulse pairs, respectively. Finally, the transmitted signal for the ith symbol $\mathbf{B}_i$ can be expressed as

$$s(t) = \sqrt{\frac{E_s}{2N_s}} \sum_{j=iN_s}^{(i+1)N_s-1} d_j[\, w_{\mathrm{tr}}(t - jT_f) + \tilde{b}_{\lfloor j/N_s \rfloor} v^m_{j-iN_s} w_{\mathrm{tr}}(t - jT_f - T_d)\,], \tag{4.2}$$

where d_j is again the polarity randomizing sequence. For simplicity, we omitted all user-specific notations here. All other parameters have same definition as in Chapter 3, except that E_s is the energy used for transmitting one symbol. Note that the time-hopping sequence has been omitted for simplicity and will be included later when we examine our system's MA capability.

While one data bit is being transmitted using N_s pulse pairs as in the standard TR scheme as well as the conventional TR scheme, additional $\log_2 M$ data bits are transmitted simultaneously. As a result, the total data rate has been increased to

$$R_s = (1 + \log_2 M) R_b, \tag{4.3}$$

compared to the data rate $R_b = 1/(N_s T_f)$ achievable by the convenional TR scheme. Furthermore, the data rate of the existing TR system is limited by the multipath delay spread because the delay between the reference and the data pulses T_d should be greater than the channel delay spread T_m, so as not to incur the interference between the reference and the data pulses in a frame. As will be shown later, our scheme is able to suppress the IPI even if T_d is less than T_m. Consequently, the system's achievable information rate can be further increased. Note that in order to maintain the code orthogonality, T_d should be at lease greater than a chip time T_c.

4.2.2 Receiver

The transmitted signal arrives at the receiver after going through the multipath channel and being corrupted by the AWGN. At the receiver, whose block diagram is shown in Fig. 4.3. the received signal, denoted by $r(t)$, first passes through a bank of $M+1$ matched filters, whose impulse responses are matched to the template signals for the ith symbol. The template signals are given by

$$h_+^{(i)}(t) = \frac{1}{\sqrt{N_s}} \sum_{j=iN_s}^{(i+1)N_s-1} d_j \, w_{\text{rec}}(t - jT_f) \tag{4.4}$$

$$h_{k-}^{(i)}(t) = \frac{1}{\sqrt{N_s}} \sum_{j=iN_s}^{(i+1)N_s-1} d_j \, v_{j-iN_s}^k \, w_{\text{rec}}(t - jT_f), \quad k = 0, 1, \ldots, M-1. \tag{4.5}$$

The corresponding matched filter outputs can be expressed as

$$y_+^{(i)}(t) = \int_{-\infty}^{+\infty} r(\tau) \, h_+^{(i)}(\tau - t) d\tau \tag{4.6}$$

$$y_{k-}^{(i)}(t) = \int_{-\infty}^{+\infty} r(\tau) \, h_{k-}^{(i)}(\tau - t) d\tau, \quad k = 0, 1, \ldots, M-1 \tag{4.7}$$

Then, $y_+^{(i)}(t)$ is delayed by T_d, multiplied with $y_{k-}^{(i)}(t)$ and then integrated over a certain time interval to yield M decision variables, given by

$$Z_k = \int_{T_d - T_c}^{T_d + QT_c} y_+^{(i)}(t - T_d) \, y_{k-}^{(i)}(t) \, dt, \quad k = 0, 1, \ldots, M-1 \tag{4.8}$$

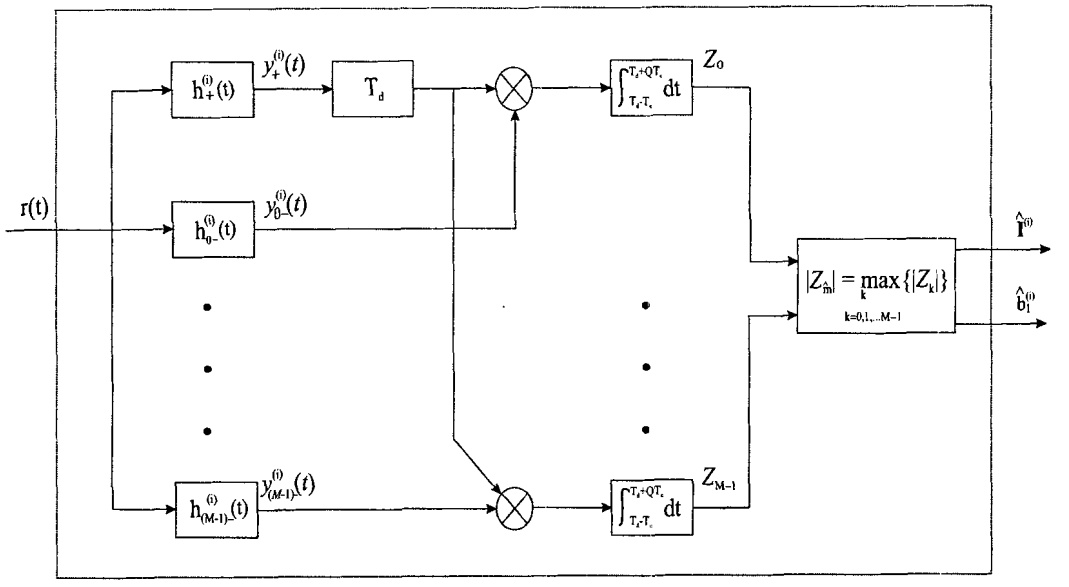

Figure 4.3: M-ary orthogonal coded/Balanced TR system: the receiver.

with $0 \leq QT_c \leq T_m$ to collect most of the signal energy spreaded over all the MPCs. Note that since we assume $T_f > T_d + T_m$ to ensure there is no IFI, only the first frame of the matched filter outputs are of interest. Then, the decision variables $\{Z_k | k = 0, 1, \ldots, M-1\}$ are compared to choose the one with the largest absolute value, denoted by

$$|Z_{\hat{m}}| = \max_{0 \leq k \leq M-1} \{|Z_k|\} \tag{4.9}$$

and finally the $1 + \log_2 M$ data bits are decoded as follows:

$$\hat{\mathbf{I}}^{(i)} = (\hat{m})_2 \tag{4.10}$$

$$\hat{b}_1^{(i)} = \frac{1}{2}\Big[1 + \text{sign}(Z_{\hat{m}})\Big] \tag{4.11}$$

where sign(x) equals to +1 if $x > 0$ and -1 otherwise.

4.2.3 The IPI cancellation

This receiver structure summarized above differs from the conventional TR scheme by introducing additional M matched filters whose impulse responses are also *matched* to the

M-ary orthogonal codes. Especially, by conforming to the abovementioned two design criterions, the receiver is able to cancel out the IPI resulted from the multipath as well as achieve M-ary orthogonal modulations. The IPI cancellation mechanism is shown in Fig. 4.4, where we assume $N_s = 4$, $\mathbf{V}^m = (1, -1, 1, -1)$, $b_1^{(i)} = 1$ and $d_j = (1, 1, 1, 1)$ have been used.

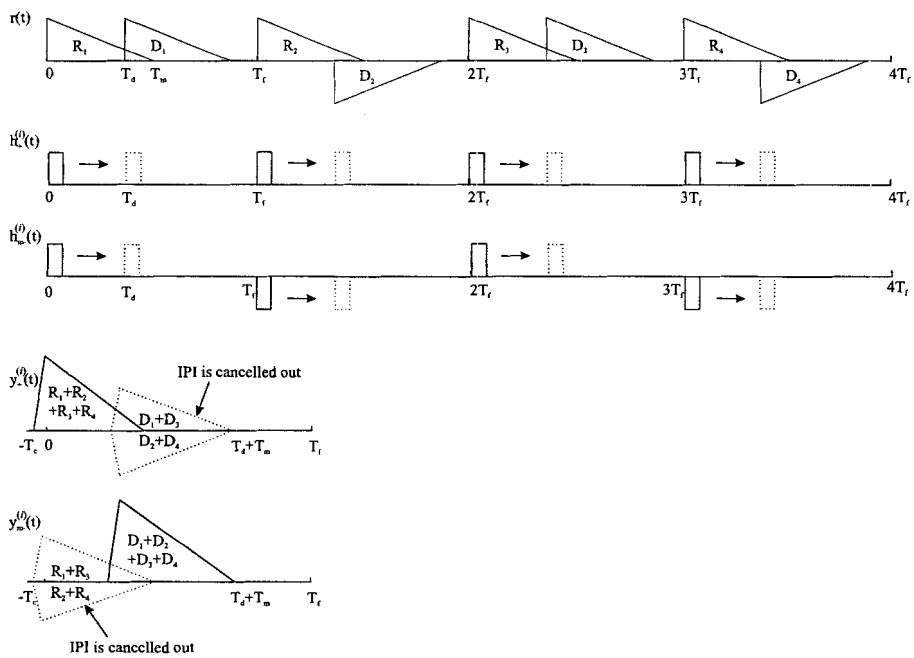

Figure 4.4: the IPI cancellation mechanism of the proposed system.

In Fig. 4.4, R_n and D_n represent the received reference and data waveforms in the nth frame, respectively. As can be seen in the first sub-figure, the tail portion of each reference waveform is overlapped with its associated data waveform. The filtering process is shown in the second and third sub-figures. As the template signals $h_+^{(i)}(t)$ and $h_{m-}^{(i)}(t)$ are shifted and correlated with the received waveform, there will be IPIs occurred in the filter outputs $y_+^{(i)}(t)$ and $y_{m-}^{(i)}(t)$, shown by the dotted lines in the last two sub-figures, respectively. However, it is easy to find that due to the adoption of the code sequence $\mathbf{V}^m$ with equal numbers of +1 and -1, the IPIs in N_s frames are added *destructively*, thus fully cancelled out. Note that, in order to perfectly eliminate the IPI, the multipath channel is assumed to be at least

invariant over one symbol duration, which is easily satisfied in the high-data-rate UWB communications.

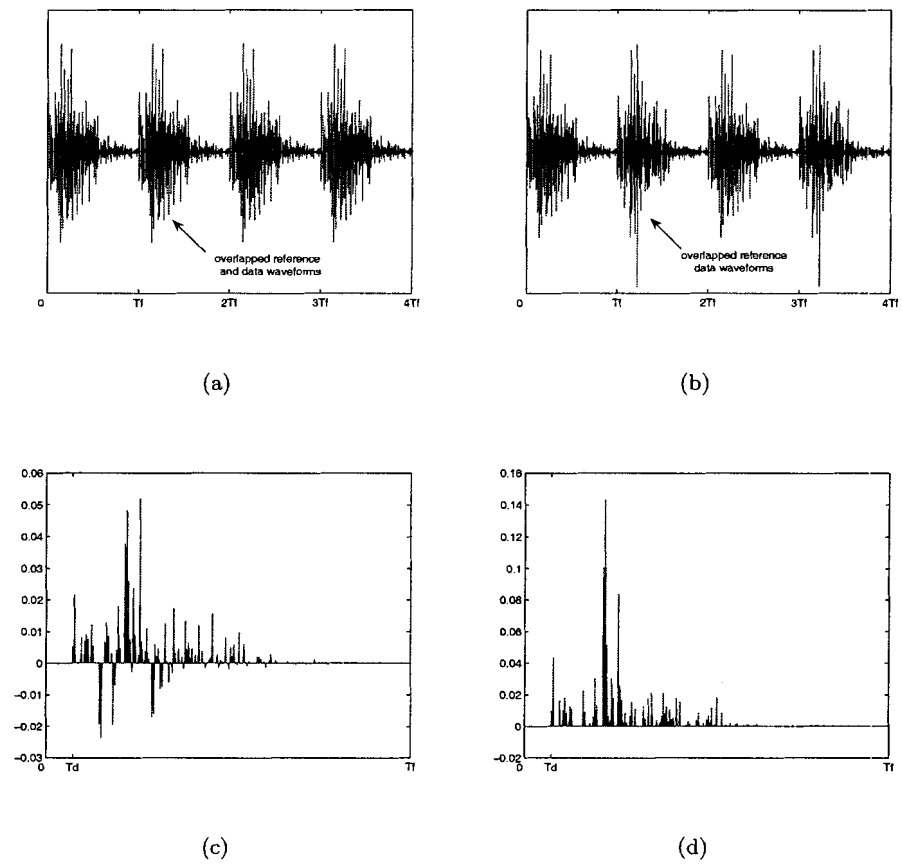

Figure 4.5: (a), (b) are the received waveforms; (c), (d) are the correlator inputs; for the conventional and the proposed TR systems, respectively

To better examine our scheme's IPI cancellation mechanism and compare with the conventional TR scheme, Fig. 4.5 (a) and (b) plot two noise-free received waveforms for the two systems, respectively, using the same parameters, i.e. $\{N_s, \mathbf{V}^m, b_1^{(i)}\}$, as Fig. 4.4. The two systems are assumed to be under the same channel condition and the distance between the reference and the data pulses T_d is less than the channel delay spread T_m. Note that in

the convention TR system, no orthogonal code is used and there is only one matched filter $h_{+}^{(i)}(t)$. The outputs of the multipliers, which are also the inputs to the correlators, in two systems are shown in Fig. 4.5 (c) and (d), respectively. It can be seen that in our proposed TR system, the MPCs share the same polarity determined by $b_1^{(i)}$, thus can be coherently integrated for detecting the data; while the conventional TR system suffers from the IPI and leads to non-coherently integrating the MPCs with different polarities.

In summary, each of these M matched filters $\{h_{m-}^{(i)}(t)|m = 0, 1, \ldots, M-1\}$, coupled with $h_{+}^{(i)}(t)$, forms a pair of said *balanced* matched filters. The mth pair of balanced matched filters is able to eliminate the IPI for the signals that have been transmitted using the code $\mathbf{V}^m$. Furthermore, due to the orthogonality among different codes, the outputs of other matched filters, which are not matched to the code that has been used by the transmitter, simply become zero. This enables the M-ary orthogonal modulation. As mentioned early, if $M = 1$ is used, no additional data bit will be sent. However, we still use a fixed code which meets the first design criterion for enabling the IPI cancellation mechanism. This special embodiment is referred to as Balanced TR system, as compared to M-ary orthogonal/Balanced TR system.

4.3 Performance Analysis

In this section, we provide a detailed performance analysis for the proposed system. Specifically, we compare the proposed TR systems with the conventional TR system in terms of the achievable information rate, subject to a target BER. Analytical approach is adopted by deriving the symbol-error-rate (SER) or BER for the M-ary orthogonal coded/Balanced TR or the Balanced TR system. Since there is no pure analytical solution for the channel-averaged SER or BER available, we will still use a semi-analytical/simulation approach to carry out our analysis.

4.3.1 Derivation of SER

Since the binary scheme is a special case of the bi-orthogonal scheme, we first derive the SER for an M-ary orthogonal/balanced TR system. The BER expression for the balanced TR system can thus be obtained by setting $M = 1$ accordingly. The received signal for the ith symbol $\mathbf{B}_i$, assuming the orthogonal code $\mathbf{V}^m$ has been used without loss of generality,

can be expressed as

$$r(t) = \sqrt{\frac{E_s}{2N_s}} \sum_{j=iN_s}^{(i+1)N_s-1} d_j \left[g(t - jT_f - c_jT_c) + \tilde{b}_{\lfloor j/N_s \rfloor} v^m_{j-iN_s} g(t - jT_f - T_d - c_jT_c) \right] + n(t) \tag{4.12}$$

Then, the outputs of the matched filter bank can be written as

$$y^{(i)}_{+}(t) = \int r(\tau) h^{(i)}_{+}(\tau - t)\, d\tau = \sum_{j=iN_s}^{(i+1)N_s-1} \lambda_j(t) \tag{4.13}$$

$$y^{(i)}_{k-}(t) = \int r(\tau) h^{(i)}_{k-}(\tau - t)\, d\tau = \sum_{j=iN_s}^{(i+1)N_s-1} v^k_{j-iN_s} \lambda_j(t), \tag{4.14}$$

where $k = 0, 1, \ldots, M-1$. Based on the assumption that $T_f \geq N_hT_c + T_d + T_m$ (i.e., assuming no IFI), the jth frame's contribution $\lambda_j(t)$ has the expression

$$\lambda_j(t) = \frac{1}{N_s}\sqrt{\frac{E_s}{2}} \left[\Lambda(t) + \tilde{b}_{\lfloor j/N_s \rfloor} v^m_{j-iN_s} \Lambda(t - T_d) \right] + \frac{1}{\sqrt{N_s}} n_j(t). \tag{4.15}$$

where $\Lambda(t)$ is the waveform correlation function, defined by $\Lambda(t) = g(t) \otimes w_{\text{rec}}(-t)$, and the jth frame's filtered noise is

$$n_j(t) = d_j \int_{-\infty}^{\infty} n(\tau) w_{\text{rec}}(\tau - t - jT_f - c_jT_c)\, d\tau \tag{4.16}$$

By substituting (4.13) and (4.14) into (4.8), the output of the kth integrator is of the form

$$Z_k = \sum_j \sum_{j'} v^k_{j'-iN_s} \int_{T_d-T_c}^{T_d+QT_c} \lambda_j(t - T_d) \lambda_{j'}(t)\, dt = \xi_k + N_1 + N_2 \tag{4.17}$$

where we have omitted the summation limit for j and j' for notational simplicity. In (4.17), ξ_k is the desired signal term, whereas N_1 and N_2 represent the noise-times-noise and the signal-times-noise terms, respectively. It is easy to verify that N_1 and N_2 are zero-mean uncorrelated random variables. The desired signal term

$$\begin{aligned} \xi_k = \left(\frac{E_s}{2N_s^2}\right) \sum_j \sum_{j'} \int_{T_d-T_c}^{T_d+QT_c} \Big[& v^k_{j'-iN_s} \Lambda(t - T_d)\, \Lambda(t) \\ & + \tilde{b}_{\lfloor j/N_s \rfloor} v^k_{j'-iN_s} v^m_{j-iN_s} \Lambda(t - 2T_d)\, \Lambda(t) \\ & + \tilde{b}_{\lfloor j'/N_s \rfloor} v^k_{j'-iN_s} v^m_{j'-iN_s} \Lambda^2(t - T_d) \\ & + \tilde{b}_{\lfloor j/N_s \rfloor} \tilde{b}_{\lfloor j'/N_s \rfloor} v^k_{j'-iN_s} v^m_{j-iN_s} v^m_{j'-iN_s} \Lambda(t - 2T_d)\, \Lambda(t - T_d) \Big] dt \end{aligned} \tag{4.18}$$

Note that $\tilde{b}_{\lfloor j/N_s \rfloor}$ and $\tilde{b}_{\lfloor j'/N_s \rfloor}$ both equal to $\tilde{b}_i$ for all j and j', respectively. By virtue of the *zero-mean averaging* due to the first code design criterion, i.e.,

$$\sum_{j'} v^k_{j'-iN_s} = 0 \quad \text{and} \quad \sum_{j} v^m_{j-iN_s} = 0,$$

as well as the *code orthogonality* due to the second code design criterion, i.e.,

$$\sum_{j'} v^k_{j'-iN_s} v^m_{j'-iN_s} = N_s \delta[k-m]$$

where $\delta[n] = 1$ if $n = 0$ and zero otherwise, ξ_k turns out to be

$$\xi_k = \tilde{b}_i \delta[k-m] \left(\frac{E_s}{2}\right) \int_{-T_c}^{QT_c} \Lambda^2(t)\, dt. \tag{4.19}$$

Note that, from (4.18) to (4.19), the 1st, 2nd and 4th terms in (4.18) have been averaged out. Next, the noise-times-noise term N_1 is written as

$$N_1 = \frac{1}{N_s} \sum_j \sum_{j'} v^k_{j'-iN_s} \int_{T_d-T_c}^{T_d+QT_c} n_j(t-T_d)\, n_{j'}(t) dt, \tag{4.20}$$

whose variance can be evaluated in Appendix B.1 (<u>with the constraint</u> $T_d \geq 2T_c$) as

$$\sigma_1^2 = \left(\frac{N_o}{2}\right)^2 \int_{-T_c}^{QT_c} \int_{-T_c}^{QT_c} R_w^2(t-s)\, dt\, ds. \tag{4.21}$$

Recall that $R_w(\cdot)$ is the autocorrelation function of the received pulse $w_{\text{rec}}(t)$. Finally, the signal-times-noise term of the kth integrator, denoted by $N_{2,k}$, is written as

$$\begin{aligned} N_{2,k} = \frac{1}{N_s}\sqrt{\frac{E_s}{2N_s}} \sum_j \sum_{j'} \int_{T_d-T_c}^{T_d+QT_c} \Big[& v^k_{j'-iN_s} \Lambda(t-T_d)\, n_{j'}(t) \\ & + \tilde{b}_{\lfloor j/N_s \rfloor} v^m_{j-iN_s} v^k_{j'-iN_s} \Lambda(t-2T_d)\, n_{j'}(t) \\ & + v^k_{j'-iN_s} n_j(t-T_d)\, \Lambda(t) \\ & + \tilde{b}_{\lfloor j'/N_s \rfloor} v^m_{j'-iN_s} v^k_{j'-iN_s} n_j(t-T_d)\, \Lambda(t-T_d) \Big] dt \end{aligned} \tag{4.22}$$

Again, by virtue of the zero-mean averaging, it follows that

$$\begin{aligned} N_{2,k} = \frac{1}{N_s}\sqrt{\frac{E_s}{2N_s}} \sum_j \sum_{j'} \int_{T_d-T_c}^{T_d+QT_c} \Big[& v^k_{j'-iN_s} \Lambda(t-T_d)\, n_{j'}(t) \\ & + \tilde{b}_{\lfloor j'/N_s \rfloor} v^m_{j'-iN_s} v^k_{j'-iN_s} n_j(t-T_d)\, \Lambda(t-T_d) \Big] dt \end{aligned} \tag{4.23}$$

where the 2nd and 3rd terms in (4.22) have been averaged out. Hence, the variance of $N_{2,k}$ can be evaluated in Appendix B.2 as

$$\sigma_{2,k}^2 = \Big\{1 + \delta[k-m]\Big\}\left(\frac{N_o E_s}{4}\right)\int_{-T_c}^{QT_c}\int_{-T_c}^{QT_c} \Lambda(t)\,\Lambda(s)\,R_w(t-s)\,dt\,ds. \tag{4.24}$$

Since the M-ary orthogonal coded/balanced TR signaling can be viewed as a *bi-orthogonal* scheme, if the composite of the two uncorrelated noise terms N_1 and N_2 can be modeled as a Gaussian random variable,[2] the SER is formulated as [36]

$$\begin{aligned} P(\epsilon) &= 1 - \Pr\left[\bigcap_{k\neq m} |Z_k| < Z_m \,\middle|\, \tilde{b}_i = 1,\, \mathbf{V}_m\right] \\ &= 1 - \int_0^\infty \left[1 - 2Q\left(\frac{x}{\sqrt{\sigma_1^2+\sigma_{2,k}^2}}\right)\right]^{M-1} \phi\left(\frac{x-\xi_m}{\sqrt{\sigma_1^2+\sigma_{2,m}^2}}\right) dx \end{aligned} \tag{4.25}$$

where $\mathbf{E}\{Z_k Z_{k'}\} = 0$ $(k \neq k' \neq m)$ and $\mathbf{E}\{Z_k(Z_m - \xi_m)\} = 0$ because of a set of the orthogonal sequences (i.e., $\{Z_k\}$ are statistically independent), $\mathbf{V}_m$ denotes the mth code carrying additional $\log_2 M$ bits via M-ary orthogonal coded TR signaling, and $Q(x/\sigma) = \int_x^\infty \phi(u/\sigma)\,du$ for $\phi(u/\sigma) = 1/\sqrt{2\pi\sigma^2}\exp(-u^2/2\sigma^2)$. By defining the *equivalent* output SNR for the desired signal as

$$\gamma = \frac{\xi_m^2}{\sigma_1^2 + \sigma_{2,m}^2},$$

the SER is further simplified into the form

$$P(\epsilon) = 1 - \int_0^\infty [\,1 - 2Q(\sqrt{\rho}z)\,]^{M-1}\phi(z - \sqrt{\gamma})\,dz \tag{4.26}$$

where $Q(x)$ and $\phi(u)$ are obtained from $Q(x/\sigma)$ and $\phi(u/\sigma)$ by letting $\sigma = 1$, and

$$\rho = \frac{\sigma_1^2 + \sigma_{2,m}^2}{\sigma_1^2 + \sigma_{2,k}^2} \geq 1 \qquad (k \neq m)$$

because of $\sigma_{2,m}^2 = 2\,\sigma_{2,k}^2$ in (4.24). Also note that the BER for the balanced TR signaling is found in (4.26) by substituting $M = 1$.

The final expression on $P(\epsilon)$ in (4.26) does not depend on a specific delay T_d between the two pulses, which implies that $T_d = \Delta T_c$ can be chosen to the minimum value $T_d = 2T_c$ (i.e., $\Delta = 2$) for a maximum achievable data rate. Given the constraint $T_d \geq T_m$ to have

[2]In fact, if the integration interval (i.e., Q) is sufficiently large, N_1 approaches the Gaussian noise, while the linear filtered term N_2 becomes Gaussian. Thus, the total noise $N_1 + N_2$ is approximately Gaussian.

zero IPI for the conventional TR signaling, where $T_f \geq T_c + T_d + T_m \geq T_c + 2T_m$ with no TH shift assumed (i.e., $N_h = 1$) for a single-user TR, the information rate is ideally increased to

$$R_s^* = (1 + \log_2 M) R_b \left(\frac{T_c + 2T_m}{3T_c + T_m} \right) \tag{4.27}$$

for M-ary orthogonal coded/balanced TR signaling.

4.3.2 Timing jitter

In practice, the UWB pulse transmission suffers from timing jitter because of the very narrow pulses and the time dispersion of the pulse energy due to dense multipath. In this situation, we should take into account the random timing jitters resulting from clock instability and tracking errors [30], along with relative motion between transmitter and receiver. We use ε_j and $\varepsilon_{j,d}$ to represent the timing jitters of the filtered output and the T_d seconds delayed filtered output in jth frame, respectively. Here, ε_j and $\varepsilon_{j,d}$ are assumed to be uniformly distributed over a fraction of chip time T_c, i.e., $[-\kappa T_c, \kappa T_c]$ for $\kappa < 1$ and uncorrelated random variables.[3]

To analyze the effect of timing jitter on the SER performance, the filtered output and the T_d seconds delayed filtered output, i.e., $\lambda_j(t)$ and $\lambda_{j'}(t - T_d)$ in (4.17) are modeled as $\lambda_j(t - \varepsilon_j)$ and $\lambda_{j'}(t - T_d - \varepsilon_{j',d})$ in characterizing the decision statistics $\{Z_k\}$. With non-zero timing jitters, there will exist *residual* IPIs due to imperfect cancellation which will degrade the system SER performance.

First, the desired term ξ_k in (4.18) consists of mean μ_k and zero-mean random variable $\xi_{k,\varepsilon}$ due to the residual IPI, where the latter is assumed to be Gaussian distributed for large values of N_s [31]. Then, the mean and the variance of $\xi_{k,\varepsilon}$ are evaluated in Appendix B.3 as

$$\mu_k = \tilde{b}_i \delta[k - m] \left(\frac{E_s}{2} \right) \int_{-T_c}^{QT_c} \left[\overline{\Lambda(t - \varepsilon)} \right]^2 dt \tag{4.28}$$

$$\begin{aligned} \sigma_{\xi_{k,\varepsilon}}^2 = & \left(\frac{E_s^2}{4N_s^2} \right) \int_{-T_c}^{QT_c} \int_{-T_c}^{QT_c} \left[\varphi(t + T_d, s + T_d) + \varphi(t, s) + N_s \delta[k - m] \overline{\Lambda(t - \varepsilon)}\, \overline{\Lambda(s - \varepsilon)} \right] \\ & \times \left[\varphi(t, s) + \varphi(t - T_d, s - T_d) + N_s \overline{\Lambda(t - \varepsilon)}\, \overline{\Lambda(s - \varepsilon)} \right] dt\, ds - \mu_k^2 \end{aligned} \tag{4.29}$$

[3]If the timing jitters appear partially correlated within a frame, the analysis made in this thesis will present somewhat optimistic results.

where $\varphi(t,s) \triangleq \overline{\Lambda(t-\varepsilon)\Lambda(s-\varepsilon)} - \overline{\Lambda(t-\varepsilon)}\,\overline{\Lambda(s-\varepsilon)}$ with $\overline{X} = \mathbf{E}\{X\}$ for notational simplicity. Note that as ε goes to zero, $\lim_{\varepsilon\to 0}\varphi(t,s) = 0$, which means $\lim_{\varepsilon\to 0}\sigma^2_{\xi_{k,\varepsilon}} = 0$ (i.e., zero residual IPI).

Next, the noise-times-noise term N_1 remains statistically the same as that without timing jitter since the linear filtered noise $n_j(t)$ in (4.16) is a stationary Gaussian random process. Meanwhile, the signal-times-noise term N_2 is zero-mean Gaussian but involves the excess variance due to the residual IPI, whose variance is evaluated (similarly in Appendix C) as

$$\begin{aligned}\sigma^2_{2,k} &= \bar{\sigma}^2_{2,k} + \left(\frac{N_o E_s}{4N_s}\right)\int_{-T_c}^{QT_c}\int_{-T_c}^{QT_c} R_w(t-s)\Big[\varphi(t+T_d, s+T_d) \\ &\quad + 2\varphi(t,s) + \varphi(t-T_d, s-T_d)\Big]\,dt\,ds. \end{aligned} \tag{4.30}$$

In the above the *mean-sense* variance $\bar{\sigma}^2_{2,k}$ is given by (4.24) with $\Lambda(t)$ and $\Lambda(s)$ replaced by $\mathbf{E}[\Lambda(t-\varepsilon)]$ and $\mathbf{E}[\Lambda(s-\varepsilon)]$, that is,

$$\bar{\sigma}^2_{2,k} = \Big\{1+\delta[k-m]\Big\}\left(\frac{N_o E_s}{4}\right)\int_{-T_c}^{QT_c}\int_{-T_c}^{QT_c}\overline{\Lambda(t-\varepsilon)}\,\overline{\Lambda(s-\epsilon)}R_w(t-s)\,dt\,ds. \tag{4.31}$$

Note that if we let $\sigma^2_{2,k} = \bar{\sigma}^2_{2,k} + \sigma^2_{2,\varepsilon}$ in (4.30) for the *excess* variance $\sigma^2_{2,\varepsilon}$ and let ε go to zero, then $\lim_{\varepsilon\to 0}\varphi(t,s) = 0$, leading to $\lim_{\varepsilon\to 0}\sigma^2_{2,\varepsilon} = 0$ (i.e., zero residual IPI).

Since the residual IPI is assumed to be Gaussian distributed, the SER with timing jitter can be found in (4.26), if we substitute

$$\begin{aligned}\rho(T_d) &= \frac{\sigma^2_{\xi_{m,\varepsilon}}(T_d) + \sigma^2_1 + \bar{\sigma}^2_{2,m} + \sigma^2_{2,\varepsilon}(T_d)}{\sigma^2_{\xi_{k,\varepsilon}}(T_d) + \sigma^2_1 + \bar{\sigma}^2_{2,k} + \sigma^2_{2,\varepsilon}(T_d)} \geq 1 \qquad (k \neq m) \\ \gamma(T_d) &= \frac{\mu^2_m}{\sigma^2_{\xi_{m,\varepsilon}}(T_d) + \sigma^2_1 + \bar{\sigma}^2_{2,m} + \sigma^2_{2,\varepsilon}(T_d)}\end{aligned}$$

for the two parameters ρ and γ, respectively. Here, we have explicitly indicated dependence of the two parameters on a specific delay T_d via the excess variances due to the residual IPI namely, $\sigma^2_{\xi_{k,\varepsilon}}(T_d)$ and $\sigma^2_{2,\varepsilon}(T_d)$. With timing jitter, the maximum achievable information rate, where (4.27) corresponds to that for the single-user TR with no timing jitter, is then determined as

$$R^*_s = (1+\log_2 M)R_b\left(\frac{T_c + 2T_m}{T_c + T_d + T_m}\right) \tag{4.32}$$

for M-ary orthogonal coded/balanced TR signaling.

4.4 Performance Results

Within this section only, we will refer to M-ary orthogonal coded/Balanced TR system as M-ary/Balanced TR system for notational simplicity. We have used the IEEE 802.15.3a channel models [33] and without loss of generality, will only present the results for CM1, which represents an LOS channel model. We will use the same discrete-time equivalent channel model as in Chapter 3. To verify the semi-analytical results we have derived in Section 4.3, we selected 100 best channel realizations of CM1 to get average SER or BER curves. For each channel realization, the total number of time bins is chosen to be 200 to capture most of the signal energy, as shown in Table 3.1. The received pulse is assumed to be the second-order derivative of Gaussian pulse with a pulse width of 0.167 ns. The frame time T_f is selected accordingly to ensure zero IFI. Since our focus is to demonstrate the superior performance of our proposed system and to somehow simplify the simulations, we have chosen the integration time $QT_c = 50$ chips over the entire considered input SNR range rather than optimizing it with respect to different input SNRs as mentioned in Chapter 3. First, the theoretical SER performance is validated in Fig. 4.6 for the M-ary/Balanced

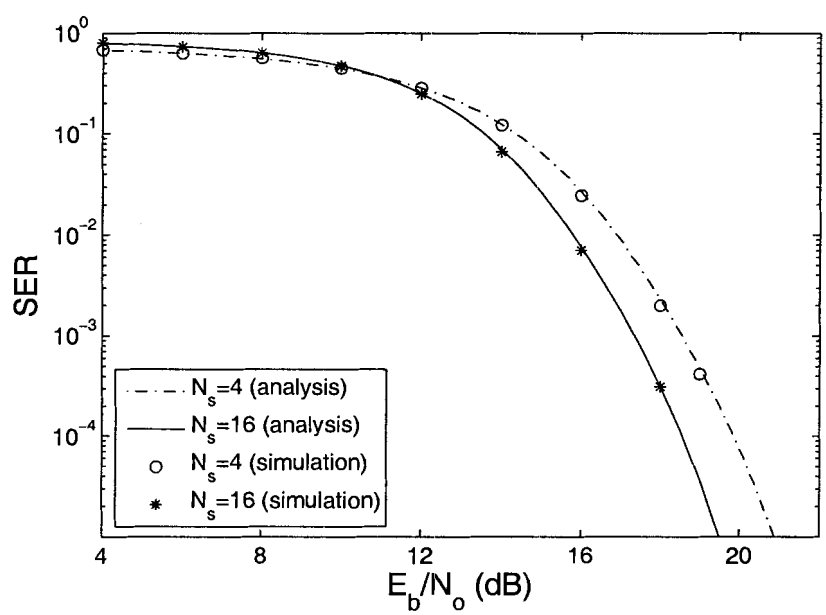

Figure 4.6: SER versus per-bit SNR for the M-ary/Balanced TR system.

TR systems when $M = \log_2 N_s = 2, 4$ for $N_s = 4, 16$. It is seen that $M = 4$-ary scheme provides about 1 dB gain over binary ($M = 2$) orthogonal one in high per-bit SNR region since the symbol SNR increases with M. As the per-bit SNR decreases, we also observe that the cross-over occurs near 11 dB due to the high-order modulation, which is more sensitive to the noisy channel. To validate the analysis carried out in Section 4.3, we also present the simulation results which fit well the corresponding theoretical ones.

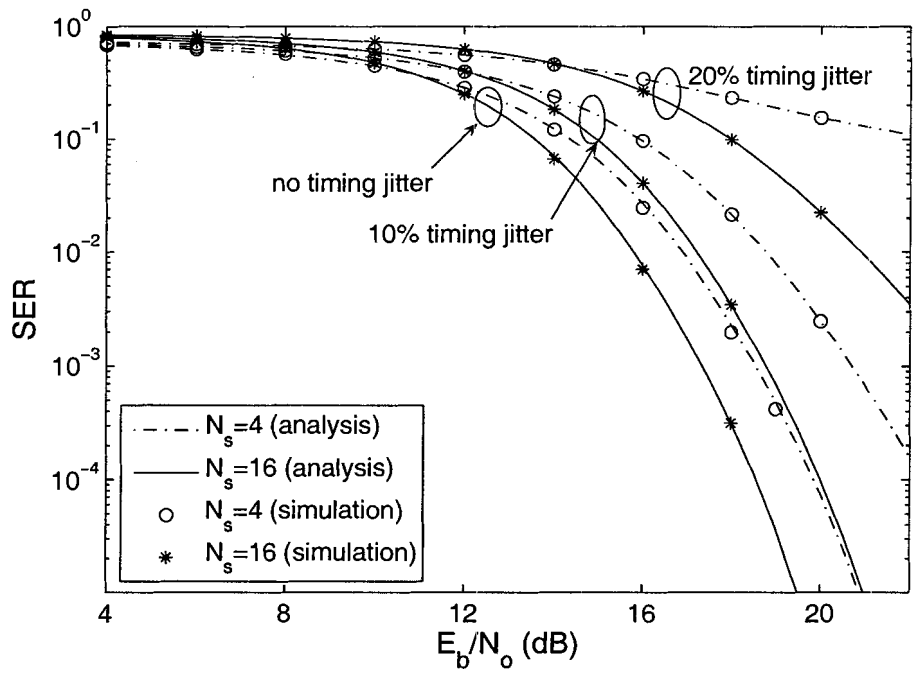

Figure 4.7: SER degradation with timing jitters for the M-ary/Balanced TR systems, when $T_d = 16$ chips.

Fig. 4.7 shows the receiver sensitivity to timing jitter for the M-ary/Balanced TR systems, in terms of the SER with $T_d = 16$ chips, when there is no timing jitter, 10% and 20% (out of the chip duration T_c) timing jitters. Considering that the typical timing jitter in UWB systems is within 15 ps [30], our timing jitter cases provide meaningful results. It is obvious that the performance degradation is considerably increasing with timing jitter, which demonstrates that the timing jitter has an adverse effect on the performance of a short-pulse-based UWB transmission. Also, the processing gain (defined as the number

of frames per symbol × the number of chips per frame) is a main factor to mitigate the performance degradation caused by timing jitter. This can be proved by observing that when $N_s = 16$, the M-ary/Balanced TR system performs much better than that when $N_s = 4$, for both 10% and 20% timing jitter cases. We note that the theoretical framework developed in Section 4.3 is verified well by the simulations, where the results from analysis and simulation coincide. Therefore, the preliminary analysis of the receiver sensitivity using the framework will effectively enable us to optimize the key system parameters in a well-defined manner.

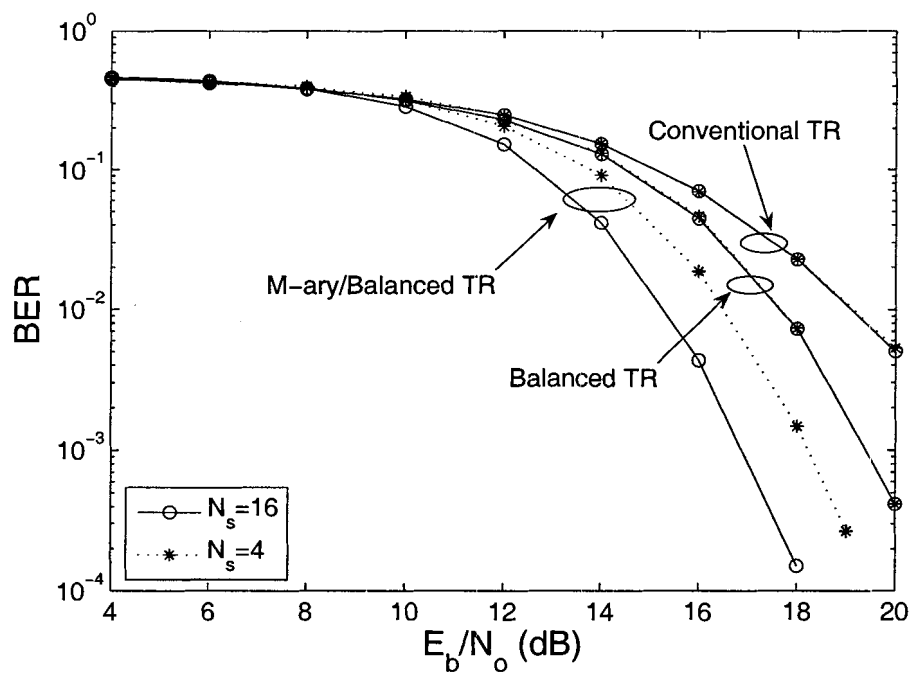

Figure 4.8: BER versus per-bit SNR for the M-ary/balanced TR, balanced TR and the conventional TR systems, when $T_d = 16$ chips.

We also investigate the BER performance of our proposed system via simulations. Fig. 4.8 shows the BER performances of M-ary/Balanced TR system, Balanced TR system and the conventional TR system for $\{N_s = 4, M = 2\}$ and $\{N_s = 16, M = 4\}$, respectively. Note that since the per-symbol energy E_s rather than per-pulse energy E_w has been used, increasing the number of frames N_s per symbol, equivanlently the number of pulses per symbol, does not improve BER performance for the conventional TR and Balanced TR

systems. As can be noticed, their BER curves corresponding to $N_s = 4$ and $N_s = 16$ overlap with each other. In Fig. 4.8, T_d is chosen to be 16 chips for all three systems. Compared to the channel delay spread $T_m = 200$ chips, there will be severe IPI between the reference and the data waveforms. However, using either M-ary/Balanced TR system or Balanced TR system, the IPI is fully eliminated as shown in Section 4.3. As a result, both M-ary/Balanced TR system and Balanced TR system provide better BER performances than the conventional TR system over the entire SNR region, except that M-ary/Balanced TR system performs worse than the other two at very low SNR range (below 6 dB) due to high order modulations.

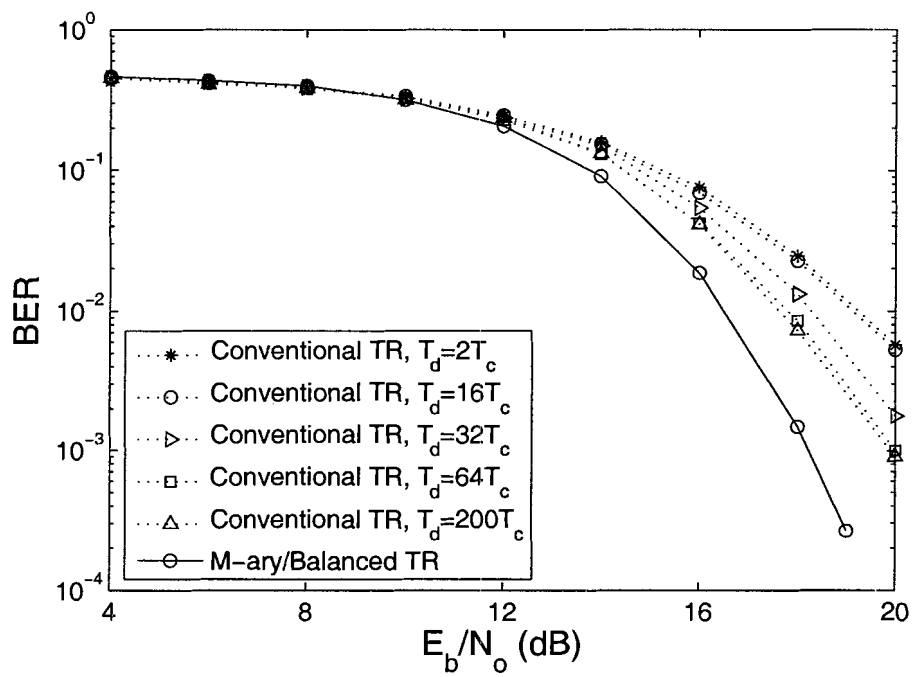

Figure 4.9: BER versus per-bit SNR for the conventional and M-ary/Balanced TR systems with respect to T_d, for $N_s = 4\,(M = 2)$, when there is no timing jitter.

In Fig. 4.9, we investigate the performance behavior of the conventional TR with respect to the time delay T_d, in order to show how the IPI affects the performance of the conventional TR system, thus highlights the advantages of our proposed system. Therefore, in Fig. 4.9, we also include the BER performance of the M-ary/Balanced TR system. Note that since

the proposed M-ary/Balanced TR system is able to fully eliminate the IPI, its performance remains unchanged for different values of T_d. Hence, we have only provided one BER curve for $T_d = 16$ chips and the other BER curves will actually overlap with this curve. From Fig. 4.9, several observations can be easily made. First, the BER performance of the conventional TR system is severely degraded as T_d decreases, because the IPI is growing inversely with T_d. To the contrary, our proposed system is robust against the changes in T_d. Second, it is interesting to see that the BER of the conventional TR does not degradate much as T_d decreases from $T_d = 200$ chips to $T_d = 64$ chips. This means in the conventional TR system, separating the reference and the data pulses at a distance larger than $T_d = 64$ chips, equivalent to about 10 ns, only leads to negligible BER improvements, because most channel energy arrives within the first 10 ns.

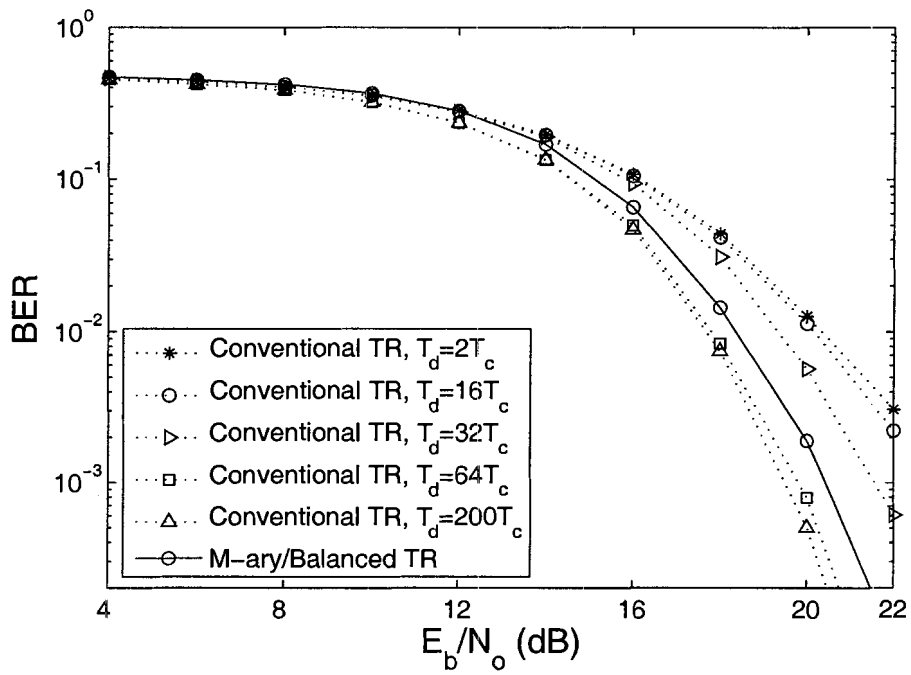

Figure 4.10: BER versus per-bit SNR for the conventional and M-ary/Balanced TR systems with respect to T_d, for $N_s = 4\,(M = 2)$, when there exists 10% timing jitter.

In Fig. 4.10, we examine the BER performances of the M-ary/Balanced TR and the conventional TR systems, when there exisits 10% timing jitter, with respect to different

values of T_d. As mentioned in Section 4.3, in the presence of timing jitter, the IPI can not be perfectly cancelled out even with the M-ary/Balanced TR system. However, our simulation results show that the BER performances of the M-ary/Balanced TR system do not change with respect to T_d. So, we only provided one BER curver correpsonding to $T_d = 16$ chips as in Fig. 4.9. As can be seen from Fig. 4.10, the per-bit SNR gain of the M-ary/Balanced TR over the conventional TR (at the target BER of 10^{-2}) is reduced for all delays T_d. In addition, the M-ary/Balanced TR performs worse than the conventional TR when $T_d > 64$ chips. This is mainly because the residual IPI degrades the performance of high-order modulation systems (our proposed TR system) more than it does the binary modulation scheme (the conventional TR system).

Another important characteristic of our proposed system is the information rate increase it has provided. In Table 4.1, we present the achievable information rate increase offered by $M = 2$-ary/Balanced TR system with $T_d = 2T_c$, relative to the conventional TR system with different values of T_d. It is obvious that we can trade the per-bit SNR gain with a

Table 4.1: Information rate increase offered by $M = 2$-ary/Balanced TR system relative to the conventional TR whose delay T_d varies from $2T_c$ to $T_m = 200T_c$ (target BER 10^{-2}).

T_d	$2T_c$	$16T_c$	$32T_c$	$64T_c$	$128T_c$	$200T_c$
Info. rate increase	R_b	$1.14R_b$	$1.30R_b$	$1.61R_b$	$2.24R_b$	$2.95R_b$
SNR gain in dB (no timing jitter)	2.74	2.64	1.79	1.31	1.15	1.13
SNR gain in dB (10% timing jitter)	1.97	1.79	0.97	-0.56	-0.62	-0.68

higher information rate, for instance, about 3 times higher information rate increase (i.e., $2.95R_b$) at 1.13 dB gain, compared to the rate increase by R_b at 2.74 dB gain when there is no timing jitter. With 10% timing jitter, the proposed TR scheme is slightly worse than the conventional TR, with a per-bit SNR penalty of -0.68 dB at a $2.95R_b$ data rate; while performs better at a R_b data rate by providing a per-bit SNR gain of 1.97 dB. Thus, the proposed M-ary balanced TR systems provides a useful design trade-off between the data rates and SNR gains.

4.5 Conclusion

In this chapter, we have introduced a novel M-ary orthogonal coded/Balanced TR system in which the inter-frame interference can be avoided because the frame time can be prolonged due to M-ary signaling as far as the required information rate is achieved. Based on this signaling approach, the inter-pulse interference has been fully eliminated by using *balanced* matched filters, which subtracts out the overlapped portion between multipath-delayed tail of the reference pulse and the subsequent information-bearing data pulse. The effective suppression of the IPI has been validated through the theoretical analysis and simulations, performed even in the presence of timing jitter. Especially, the maximum *achievable* information rate increase that results from using a shorter time delay between the two pulses, is evaluated under a theoretical framework developed to derive the SER for the M-ary orthogonal code/Balanced TR system, both without and with timing jitter. It has been shown that the usage of the proposed TR system can result in significant information rate increases even at a lower transmit power, while maintaining its superior BER performance compared to the conventional TR system. It is to be noted that the performance improvements are achieved with a modest increase in the system complexity, i.e., additional matched filters. However, as can be seen from the performance results we have presented in this chapter, the proposed system have already promised considerable information rate increase and BER improvements, with only slightly increased system complexity, e.g., $M = 2$.

Chapter 5

Conclusions and Future works

5.1 Conclusions

In the first part of this thesis, we developed a theoretical framework to analyze the performance of a UWB Rake receiver in the presence of both multipath and multiuser interference, in terms of its channel-averaged output SINR. The closed-form expression we have derived incorporated all the channel model parameters and can thus be used to directly examine or compare the performances of UWB Rake receivers in different indoor environments, i.e., CM1 to CM4. We also found that without much changing the essence of the IEEE 802.15.3a channel models, the derivation of a closed-form expression for the channel-averaged BER is intractable. In addition, using the developed theoretical framwork, we were also able to analyze the channel-averaged SINR for a UWB-TR system. A direct application of our work is to analytically determine the optimum integration interval for a UWB-TR receiver, which was usually done via simulations. Besides, we have examined the dependency of the optimum integration interval on the input SNR as well as multiple access interference. In either case, our analytical work is able to directly determine this optimum integration time without resorting to tedious simulation works.

The performance results presented in the first part of this thesis suggested that the performance degradations associated with TR system have to be considered before it is widely adopted for indoor high-data-rate UWB communications. Consequently, the second part of this thesis focused on how to improve the performance of a UWB-TR system. Specifically, we proposed a novel M-ary orthogonal coded/Balanced TR system. It has been shown, via both analyses and simulations, that the proposed system is able to fully eliminate the

inter-pulse interference occurred when the reference and the data pulses are separated at a distance less than the channel delay spread. This is especially important when UWB-TR is applied to high-data-rate communications. The performance comparisons between the proposed TR system and the conventional TR system showed that, the proposed M-ary orthogonal coded/Balanced TR system can operate at higher information rates even with lower transmit power, while maintaining its superior BER performance over the conventional TR system. We have further investigated both systems' performance in the presence of timing jitter. It has been shown that, when there exists timing jitter, the proposed system has a more stable performance with respect to different information rates. Compared to the existing method combating the inter-pulse interference, i.e., maximum likelihood template estimation, our proposed system has a much lower complexity, while achieving higher information rates.

5.2 Future works

The research work included in this thesis can be extended in several ways. First, considering that an *exact* closed-form expression for the channel-averaged BER of a UWB Rake receiver is not derived, there may exist possible approximations which can somehow simplify the analysis. This approximation has to start with an effective but practical approximation to the underlying IEEE 802.15.3a channel models. Specifically, on the one hand, it should simplify the derivation and lead to a tractable expression of the probability density function for the combined channel gain coefficient mentioned in Chapter 3. On the other hand, it should not affect the major characteristic of the well-defined channel models, such as double-Poisson arrival models for the MPCs. If these are possible, we will be able to statistically characterize the finally decision statistic and finally derive the channel-averaged BER.

In this thesis, we have examined both UWB Rake receiving and TR systems' performance based on a discretized channel model. This channel model is accurate when the pulse width is very small, e.g., 0.167 ns as used in this thesis, since the pulse overlapping phenomenon is not that serious. However, when the pulse width is larger, e.g., greater than 0.5 ns, there will be severe pulse overlappings and the resulting pulse *distortions*. In this case, the assumption that the MPCs are resolvable at the UWB Rake receiver is not accurate and the system performance results will be different. In addition, when there is pulse distortion, it is impractical to use one template for all Rake fingers. Therefore, performance analyses

taking these into account can provide more realistic and meaningful results.

Another future research direction could be analyzing the multiple access performance of our proposed M-ary orthogonal coded/Balanced TR system. In a single-user scenario, our proposed system fully eliminates the IPI and can operate at higher information rates by separating the reference and the data pulses at a much shorter distance. However, in multiuser scenario, the interfering user signals may lie in the overlapped portion of the reference and the data waveforms, which causes most of the channel errors, and hence it is desired to properly choose an optimum delay between the two pulses, so as to minimize the effect of MAI, while providing as high information rate as possbile. For this, an exact analysis of the MAI, showing how it is dependent on the delay between the reference and the data pulses, is necessary and will be one of our future research topics.

Appendix A

A.1 Evaluation of $P_q^{(n)}$

Case 1: for $q = 1$, we always have the first cluster ($l = 0$) arrived in the first time bin. The probability that this cluster has a ray contribution to the nth time bin is calculated to be

$$\begin{aligned} P_1^{(n)} &= \sum_{k=1}^{n-1} \Pr[\tau_{k,\,0} = (n-1)\Delta\tau] \\ &= \sum_{k=1}^{n-1} P_r \binom{n-2}{k-1} P_r^{k-1}(1-P_r)^{n-k+1} \\ &= P_r. \end{aligned} \tag{A.1}$$

Case 2: for $2 \le q \le n-1$, the probability that the qth time bin has a ray contribution to the nth time bin can be derived in a similar way as

$$\begin{aligned} P_q^{(n)} &= \sum_{l=1}^{q-1} \Pr[T_l = (q-1)\Delta\tau] \sum_{k=1}^{n-q} \Pr[\tau_{k,\,l} = (n-q)\Delta\tau] \\ &= \sum_{l=1}^{q-1} \Pr[T_l = (q-1)\Delta\tau] \sum_{k=1}^{n-q} P_r \binom{n-q-1}{k-1} P_r^{k-1}(1-P_r)^{n-q-k} \\ &= P_r \sum_{l=1}^{q-1} \Pr[T_l = (q-1)\Delta\tau] \\ &= P_r \sum_{l=1}^{q-1} P_c \binom{q-1}{l-1} P_c^{l-2}(1-P_c)^{q-l} \\ &= P_c \cdot P_r. \end{aligned} \tag{A.2}$$

Case 3: for $q = n$, the probability $P_q^{(n)}$ is equivalent to the probability of a cluster arrival, which is P_c.

A.2 Evaluation of average path energy $\mathbf{E}\{A_n^{(\nu)^2}\}$

Consider the first cluster in the first time bin ($\tau_1 = 0$) that occurs with probability one, then we have

$$\mathbf{E}\{A_1^{(\nu)^2}\} = \Omega_0. \tag{A.3}$$

For the time bins other than the first one, due to our mathematical modeling, the $(n-1)$ preceding time bins may contribute ray components to the nth time bin. In addition, the nth time bin may have a cluster contribution to itself. Fig. A.1 illustrates one possible channel realization for the nth time bin, in which $\beta_{n,q}^{(\nu)}$ represents the MPC in the nth time bin contributed by the qth time bin, along with $p_{n,q}^{(\nu)}$ equiprobably taking on the value of ± 1.

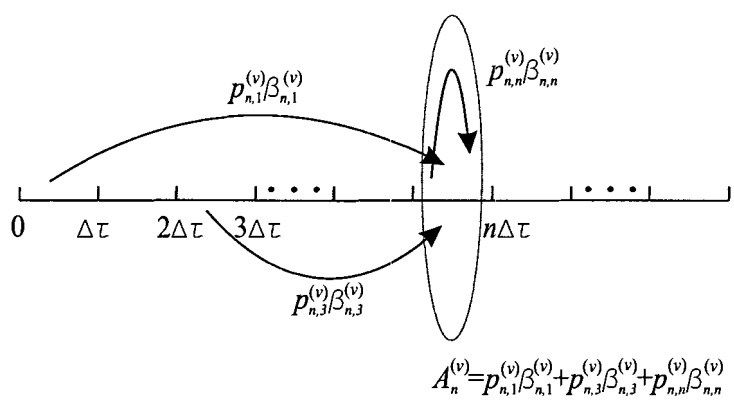

Figure A.1: One possible channel realization for nth time bin in the discrete-time channel model.

We can see that, in Fig. A.1, the first and third time bins have ray contributions to the nth time bin, and the nth time bin has a cluster contribution to itself. Recall that, in the discrete-time channel model of (3.2) the combined channel coefficient $A_n^{(\nu)}$ denotes the sum of the channel coefficients of all the MPCs in the nth time bin and this accounts for any possible *cluster overlapping*, which is an important channel characteristic of IEEE 802.15.3a channel model, especially for the NLOS channel models CM2, CM3 and CM4.

Consequently, by defining

$$U_{n,q}^{(\nu)} = \begin{cases} 1, & \text{if the } q\text{th time bin has a MPC contribution to the } n\text{th time bin} \\ 0, & \text{otherwise,} \end{cases} \tag{A.4}$$

the combined channel coefficient $A_n^{(\nu)}$ can be written as

$$A_n^{(\nu)} = \sum_{q=1}^{n} p_{n,q}^{(\nu)} \, \beta_{n,q}^{(\nu)} \, U_{n,q}^{(\nu)}. \tag{A.5}$$

When taking the expectation for ${A_n^{(\nu)}}^2$, we can use the similar relation as given in (3.12) and all the cross-terms will disappear, leading to

$$\begin{aligned} \mathbf{E}\{{A_n^{(\nu)}}^2\} &= \sum_{q=1}^{n} \mathbf{E}\left\{{p_{n,q}^{(\nu)}}^2 {\beta_{n,q}^{(\nu)}}^2 {U_{n,q}^{(\nu)}}^2\right\} \qquad (n \geq 2) \\ &= \sum_{q=1}^{n} \mathbf{E}\left\{{\beta_{n,q}^{(\nu)}}^2 {U_{n,q}^{(\nu)}}^2 \middle| U_{n,q}^{(\nu)} = 1\right\} \Pr\left[U_{n,q}^{(\nu)} = 1\right] \\ &= \sum_{q=1}^{n} \mathbf{E}\left\{{\beta_{n,q}^{(\nu)}}^2\right\} \Pr\left[U_{n,q}^{(\nu)} = 1\right] \end{aligned} \tag{A.6}$$

where the probability of $U_{n,q}^{(\nu)} = 1$ is simply $P_q^{(n)}$, which is given by the lemma 1 in (3.15). Furthermore, according to the IEEE 802.15.3a channel model [33], we have

$$\mathbf{E}\{{\beta_{n,q}^{(\nu)}}^2\} = \Omega_0 \exp\left[-\frac{(q-1)\Delta\tau}{\Gamma}\right] \exp\left[-\frac{(n-q)\Delta\tau}{\gamma}\right] \tag{A.7}$$

Substituting (3.15) and (A.7) into (A.6), then combining with (A.3), we will finally obtain (3.16).

A.3 SNR and SINR for UWB-TR systems

A.3.1 Average SNR for single-user UWB-TR system

The decision statistic of a single-user UWB-TR system, defined by (3.20), can be rewritten as

$$Z^{(1)} = \xi + N_1 + N_2 \tag{A.8}$$

where the three terms of right-hand side represent the desired signal, noise-times-signal, noise-times-noise, respectively. The desired signal energy is easily evaluated as

$$|\mathbf{E}\{\xi\}|^2 = N_s^2 E_w^2 \left[G^{(1)}(Q)\right]^2. \tag{A.9}$$

It is easy to show that N_1 and N_2 are zero-mean and independent of each other. Furthermore, the variance of N_1 is easily evaluated to be

$$\sigma_{N_1}^2 = N_s E_w N_o G^{(1)}(Q). \tag{A.10}$$

As for the noise-times-noise term, the autocorrelation function $r_n(\tau)$ for the front-end filtered noise can be expressed as

$$r_n(\tau) = N_o W \mathrm{sinc}(2W\tau). \tag{A.11}$$

According to [37], the variance for the noise-times-noise term can be calculated as

$$\sigma_{N_2}^2 = 2N_s \int_0^{T_{\mathrm{corr}}} (T_{\mathrm{corr}} - \tau) r_n^2(\tau)\, d\tau. \tag{A.12}$$

Substituting (A.11) into (A.12), we obtain

$$\begin{aligned}\sigma_{N_2}^2 &= 2N_s N_o^2 W^2 \int_0^{T_{\mathrm{corr}}} (T_{\mathrm{corr}} - \tau)\, \mathrm{sinc}^2(2W\tau)\, d\tau \\ &= N_s N_o^2 W T_{\mathrm{corr}} \int_0^{2WT_{\mathrm{corr}}} \mathrm{sinc}^2(t)\, dt + \frac{1}{2} N_s N_o^2 \int_0^{2WT_{\mathrm{corr}}} t\, \mathrm{sinc}^2(t)\, dt. \end{aligned} \tag{A.13}$$

Typically, WT_{corr} is very large, in which case the first term in (A.13) can be approximated to

$$N_s N_o^2 W T_{\mathrm{corr}} \int_0^{2WT_{\mathrm{corr}}} \mathrm{sinc}^2(t)\, dt \approx \frac{1}{2} N_s N_o^2 W T_{\mathrm{corr}}. \tag{A.14}$$

For the second term in (A.13), we can bound it as

$$\begin{aligned}\frac{1}{2} N_s N_o^2 \int_0^{2WT_{\mathrm{corr}}} t\, \mathrm{sinc}^2(t)\, dt &= \frac{1}{2} N_s N_o^2 \left[\int_0^1 t\, \mathrm{sinc}^2(t)\, dt + \int_1^{2WT_{\mathrm{corr}}} t\, \mathrm{sinc}^2(t)\, dt \right] \\ &\leq \frac{1}{2} N_s N_o^2 \left[1 + \int_1^{2WT_{\mathrm{corr}}} t^2 \mathrm{sinc}^2(t)\, dt \right] \\ &= \frac{1}{2} N_s N_o^2 \left[1 + \frac{1}{2\pi^2} \int_1^{2WT_{\mathrm{corr}}} [1 - \cos(2\pi t)]\, dt \right] \\ &\approx \frac{1}{2} N_s N_o^2 + \frac{1}{2\pi^2} N_s N_o^2 W T_{\mathrm{corr}}. \end{aligned} \tag{A.15}$$

Comparing the dominant term in (A.15) with (A.14), we find that (A.14) is about 10 dB larger for a typical range. Hence, we can simply ignore the second term in (A.13), resulting in

$$\sigma_{N_2}^2 \approx \frac{1}{2} N_s N_o^2 W T_{\mathrm{corr}}. \tag{A.16}$$

Combining (A.9), (A.10) and (A.16), we will finally derive (3.22).

A.3.2 Average SINR for multiuser UWB-TR system

The decision statistic can now be rewritten as

$$Z^{(1)} = \xi + N_1 + N_2 + N_3 + N_4 + N_5 \tag{A.17}$$

where the three extra terms N_3, N_4 and N_5 represent MAI-times-signal, MAI-times-noise and MAI-times-MAI terms respectively. Note that in [14], the authors have derived the expression for SINR, given one particular channel realization. We refer to the [14, eq. (21)], by applying our framework, and will easily derive the second-order moments of N_3, N_4 and N_5 as

$$\sigma_{N_3}^2 = 4(N_u - 1)N_s E_w^2 \Psi(0) T_f^{-1} G^{(1)}(Q) \tag{A.18}$$

$$\sigma_{N_4}^2 = 2(N_u - 1)N_s E_w N_o R_w(0) Q T_c T_f^{-1} \tag{A.19}$$

$$\begin{aligned}\sigma_{N_5}^2 \approx\ & 4(N_u - 1)(N_u - 2)N_s T_f^{-2} \left[\int_0^{T_c} \int_{-y}^{T_c} R_w^2(x)\, dx\, dy \right. \\ & \left. + \int_0^{T_c} \int_{-T_c}^{T_c - y} R_w^2(x)\, dx\, dy + \Psi(0)(Q-2)T_c \right]. \end{aligned} \tag{A.20}$$

Note that (A.20) has ignored the self-MAI-times-MAI term. Finally, combining (A.9), (A.10), (A.16), (A.18), (A.19) and (A.20), the channel-averaged SINR in (3.26) follows.

Appendix B

B.1 Evaluation of σ_1^2 in (4.21)

The second-order moment of N_1 can be formulated as

$$\sigma_1^2 = \left(\frac{1}{N_s^2}\right) \sum_j \sum_{j'} \int_{T_d-T_c}^{T_d+QT_c} \int_{T_d-T_c}^{T_d+QT_c} \mathbf{E}[n_j(t)n_j(s)]\mathbf{E}[n_{j'}(t-T_d)n_{j'}(s-T_d)]\, dt\, ds \quad \text{(B.1)}$$

where we have used $\mathbf{E}[n_j(t)n_j(s)n_{j'}(t-T_d)n_{j'}(s-T_d)] = \mathbf{E}[n_j(t)n_j(s)]\,\mathbf{E}[n_{j'}(t-T_d)n_{j'}(s-T_d)]$, provided $T_d \geq 2T_c$. This is due to the following: i) if j is not equal to j', $n_j(t)$ and $n_{j'}(t-T_d)$ are independent as long as $T_d \geq T_c$, since the filtered noise has $R_{n_j}(\tau) = 0$ when $\tau \geq T_c$, given the signal bandwidth is on the order of T_c^{-1}. So are $n_j(s)$ and $n_{j'}(t-T_d)$ when t and s are confined to the interval $[T_d - T_c, T_d + QT_c]$. ii) if $j = j'$, as long as $T_d \geq 2T_c$, it is easy to show that $\mathbf{E}[n_j(t)n_j(s)n_j(t-T_d)n_j(s-T_d)]$ has only the term $\mathbf{E}[n_j(t)n_j(s)]\mathbf{E}[n_j(t-T_d)n_j(s-T_d)]$ left and all other terms become zero. Therefore, it can be written from (4.16) as

$$\begin{aligned}\sigma_1^2 &= \left(\frac{N_o^2}{4N_s^2}\right) \sum_j \sum_{j'} \int_{-\infty}^{\infty} \int_{-\infty}^{\infty} \Bigg[\int_{T_d-T_c}^{T_d+QT_c} \int_{T_d-T_c}^{T_d+QT_c} g_j(\tau - t) g_{j'}(\hat{\tau} - t + T_d) \\ &\quad \times g_j(\tau - s) g_{j'}(\hat{\tau} - s + T_d)\, dt\, ds \Bigg] d\tau\, d\hat{\tau} \end{aligned} \quad \text{(B.2)}$$

where we have assumed $n(t)$ to be the Gaussian noise input to the filter.[1] and defined

$$g_j(t) \triangleq d_j w_{\text{rec}}(t - jT_f - c_j T_c) \quad \text{(B.3)}$$

[1]If the RF front-end filter is applied as in Chapter 3, this noise model will not be accurate.

Now, if the free variable τ is shifted by T_d as $\tau \to \tau + T_d$ and also do the changes of variables inside the brackets, the above expression on σ_1^2 can be rewritten as

$$\sigma_1^2 = \left(\frac{N_o^2}{4N_s^2}\right)\sum_j\sum_{j'}\int_{-\infty}^{\infty}\int_{-\infty}^{\infty}\left[\int_{-T_c}^{QT_c}\int_{-T_c}^{QT_c} w_{\text{rec}}(\tau - t - jT_f - c_jT_c)w_{\text{rec}}(\hat{\tau} - t - j'T_f - c_{j'}T_c)\right.$$
$$\left.\times\, w_{\text{rec}}(\tau - s - jT_f - c_jT_c)w_{\text{rec}}(\hat{\tau} - s - j'T_f - c_{j'}T_c)\,dt\,ds\right]d\tau\,d\hat{\tau}. \tag{B.4}$$

Further, changing the variables as $u = \tau - jT_f - c_jT_c$ and $v = \hat{\tau} - j'T_f - c_{j'}T_c$ and interchanging the order of integration, we obtain

$$\begin{aligned}\sigma_1^2 &= \left(\frac{N_o^2}{4N_s^2}\right)\sum_j\sum_{j'}\int_{-T_c}^{QT_c}\int_{-T_c}^{QT_c}\left[\int_{-\infty}^{\infty} w_{\text{rec}}(u-t)w_{\text{rec}}(u-s)\,du\right.\\ &\quad\left.\times\int_{-\infty}^{\infty} w_{\text{rec}}(v-t)w_{\text{rec}}(v-s)\,dv\right]dt\,ds\\ &= \left(\frac{N_o}{2}\right)^2\int_{-T_c}^{QT_c}\int_{-T_c}^{QT_c} R_w^2(t-s)\,dt\,ds.\end{aligned} \tag{B.5}$$

B.2 Evaluation of $\sigma_{2,k}^2$ in (4.24)

Similarly as in Appendix B.1, we obtain

$$\begin{aligned}\sigma_{2,k}^2 &= \left(\frac{N_oE_s}{4N_s}\right)\sum_j\int_{T_d-T_c}^{T_d+QT_c}\int_{T_d-T_c}^{T_d+QT_c}\Lambda(t-T_d)\Lambda(s-T_d)\\ &\quad\times\left\{\delta[k-m]\mathbf{E}[n_j(t-T_d)n_j(s-T_d)] + \mathbf{E}[n_j(t)n_j(s)]\right\}dt\,ds\end{aligned} \tag{B.6}$$

where, in evaluating $\mathbf{E}\{N_{2,k}^2\}$ for $N_{2,k}$ in (4.23), the cross-terms have been averaged out due the zero-mean averaging. Hence, by (4.16) and (B.3)

$$\begin{aligned}\sigma_{2,k}^2 &= \left(\frac{N_oE_s}{4N_s}\right)\sum_j\int_{-\infty}^{\infty}\left[\int_{T_d-T_c}^{T_d+QT_c}\int_{T_d-T_c}^{T_d+QT_c}\Lambda(t-T_d)\Lambda(s-T_d)\right.\\ &\quad\left.\times\left\{\delta[k-m]g_j(\tau-t+T_d)g_j(\tau-s+T_d) + g_j(\tau-t)g_j(\tau-s)\right\}dt\,ds\right]d\tau.\end{aligned} \tag{B.7}$$

For the second term $g_j(\tau-t)g_j(\tau-s)$ above, we substitute $\tau \to \tau + T_d$, and then do the changes of variables inside the brackets, $\sigma_{2,k}^2$ can be evaluated as

$$\begin{aligned}\sigma_{2,k}^2 &= \left\{1+\delta[k-m]\right\}\left(\frac{N_oE_s}{4N_s}\right)\sum_j\int_{-\infty}^{\infty}\left[\int_{-T_c}^{QT_c}\int_{-T_c}^{QT_c}\Lambda(t)\Lambda(s)w_{\text{rec}}(\tau-t-jT_f-c_jT_c)\right.\\ &\quad\left.\times\, w_{\text{rec}}(\tau-s-jT_f-c_jT_c)\,dt\,ds\right]d\tau\end{aligned} \tag{B.8}$$

Similarly, doing the changes of variables as $u = \tau - jT_f - c_jT_c$ and interchanging the order of integration, we obtain

$$\begin{aligned}\sigma_{2,k}^2 &= \Big\{1+\delta[k-m]\Big\}\left(\frac{N_oE_s}{4N_s}\right)\sum_j\int_{-T_c}^{QT_c}\int_{-T_c}^{QT_c}\Lambda(t)\Lambda(s)\\ &\quad\times\left[\int_{-\infty}^{\infty}w_{\text{rec}}(u-t)w_{\text{rec}}(u-s)\,du\right]dt\,ds\\ &= \Big\{1+\delta[k-m]\Big\}\left(\frac{N_oE_s}{4}\right)\int_{-T_c}^{QT_c}\int_{-T_c}^{QT_c}\Lambda(t)\Lambda(s)R_w(t-s)\,dt\,ds. \qquad \text{(B.9)}\end{aligned}$$

B.3 Evaluation of μ_k and $\sigma^2_{\xi_{k,\varepsilon}}$ in (4.28) and (4.29)

With timing jitters, the desired term ξ_k in (4.18) can be expressed by

$$\begin{aligned}\xi_k = \left(\frac{E_s}{2N_s^2}\right)\sum_j\sum_{j'}\int_{T_d-T_c}^{T_d+QT_c}&\Big[v^k_{j'-iN_s}\Lambda(t-T_d-\varepsilon_{j,d})\,\Lambda(t-\varepsilon_{j'})\\ &+\tilde{b}_{\lfloor j/N_s\rfloor}v^k_{j'-iN_s}v^m_{j-iN_s}\Lambda(t-2T_d-\varepsilon_{j,d})\,\Lambda(t-\varepsilon_{j'})\\ &+\tilde{b}_{\lfloor j'/N_s\rfloor}v^k_{j'-iN_s}v^m_{j'-iN_s}\Lambda(t-T_d-\varepsilon_{j,d})\Lambda(t-T_d-\varepsilon_{j'})\\ &+\tilde{b}_{\lfloor j/N_s\rfloor}\tilde{b}_{\lfloor j'/N_s\rfloor}v^k_{j'-iN_s}v^m_{j-iN_s}v^m_{j'-iN_s}\Lambda(t-2T_d-\varepsilon_{j,d})\,\Lambda(t-T_d-\varepsilon_{j'})\Big]dt \qquad \text{(B.10)}\end{aligned}$$

First, the mean μ_k of ξ_k is due to the 3rd term above because the other terms are averaged out due to the balanced TR signaling, if the timing jitters $\varepsilon_{j'}$ and $\varepsilon_{j,d}$ for all j and j' can be modeled as uncorrelated when clock instability and tracking errors exist. Thus, μ_k simply reduces to (4.28).

Next, the *excess* variance $\sigma^2_{\xi_{k,\varepsilon}}$ of $\xi_{k,\varepsilon}$, where $\xi_k = \mu_k + \xi_{k,\varepsilon}$, is evaluated by taking the second-order moment of each term in (B.10) because the cross-terms are mean zero with respect to $\varepsilon_{j,d}$ and $\varepsilon_{j'}$. If we consider the second-order moment of the first term in (B.10) can be expressed as,

$$\begin{aligned}\left(\frac{E_s^2}{4N_s^4}\right)\int_{T_d-T_c}^{T_d+QT_c}\int_{T_d-T_c}^{T_d+QT_c}&\left[\sum_{j'}\sum_{n'}v^k_{j'-iN_s}v^k_{n'-iN_s}\overline{\Lambda(t-\varepsilon_{j'})\Lambda(s-\varepsilon_{n'})}\right]\\ &\times\left[\sum_j\sum_n\overline{\Lambda(t-\varepsilon_{j,d}-T_d)\Lambda(s-\varepsilon_{n,d}-T_d)}\right]dt\,ds. \qquad \text{(B.11)}\end{aligned}$$

Here, the term within first brackets is rewritten as

$$\sum_{j'}\overline{\Lambda(t-\varepsilon_{j'})\Lambda(s-\varepsilon_{j'})}+\sum_{j'}\sum_{n'\neq j'}v^k_{j'-iN_s}v^k_{n'-iN_s}\overline{\Lambda(t-\varepsilon_{j'})}\,\overline{\Lambda(s-\varepsilon_{n'})}$$

$$= N_s\overline{\Lambda(t-\varepsilon)\Lambda(s-\varepsilon)} - N_s\overline{\Lambda(t-\varepsilon)}\,\overline{\Lambda(s-\varepsilon)} + \sum_{j'}\sum_{n'} v^k_{j'-iN_s} v^k_{n'-iN_s}\overline{\Lambda(t-\varepsilon)}\,\overline{\Lambda(s-\varepsilon)}, \tag{B.12}$$

where the last term again becomes zero due to the balanced TR signaling. Similarly, considering the second-order moments of the remaining terms in (B.10), the final expression can be found as given in (4.29) after a few straightforward mathematical manipulations.

Bibliography

[1] R. A. Scholtz. Multiple access with time-hopping impulse modulation. In *Proceedings of IEEE MILCOM Conference*, pages 447–450, Oct. 1993.

[2] M. Z. Win and R. A. Scholtz. Impulse radio: How it works. *IEEE Communications Letters*, Vol. 2(2):36–38, Feb. 1998.

[3] M. Z. Win and R. A. Scholtz. Ultra-Wide bandwidth time-hopping spread-spectrum impulse radio for wireless multiple-access communications. *IEEE Transactions on Communications*, Vol. 48(4):679–691, Apr. 2000.

[4] M. Z. Win and R. A. Scholtz. On the robustness of Ultra-Wide bandwidth signals in dense mulpath environments. *IEEE Communications Letters*, Vol. 2(2):51–53, Feb. 1998.

[5] M. Z. Win and R. A. Scholtz. On the energy capture of Ultrawide Bandwidth signals in dense multipath environments. *IEEE Communications Letters*, Vol. 2(9):245–247, Sep. 1998.

[6] J. D. Choi and W. E. Stark. Performance analysis of Rake receivers for Ultra-Wideband communications with PPM and OOK in multipath channels. In *Proceedings of IEEE International Conference on Communications*, pages 1969–1973, Apr. 2002.

[7] A. Rajeswaran, V. S. Somayazulu, and J. R. Foerster. Rake performance for a pulse based UWB system in a realistic UWB indoor channel. In *Proceedings of IEEE International Conference on Communications*, pages 2879–2883, May 2003.

[8] C. K. Rushforth. Transmitted-reference techniques for random or unknown channels. *IEEE Transactions on Information Theory*, Vol. 10(1):39–42, Jan. 1964.

[9] G. D. Hingorani and J. C. Hancock. A transmitted reference system for communicating in random or unknown channels. *IEEE Transactions on Communications*, Vol. 13(3):293–301, Sep. 1965.

[10] R. T. Hoctor and H. W. Tomlinson. An overview of delay-hopped transmitted-reference RF communications. in Technical Information Series: G.E. Research and Development Center, Jan. 2002.

[11] J. D. Choi and W. E. Stark. Performance of Ultra-Wideband communications with suboptimal receivers in multipath channels. *IEEE Journal on Selected Areas in Communications*, Vol. 20(9):1754–1766, Dec. 2002.

[12] S. Franz and U. Mitra. Integration interval optimization and performance analysis for UWB transmitted reference systems. In *Proceedings of IEEE Conference on Ultra Wideband Systems and Technologies, joint with International Workshop on Ultra Wwideband systems*, volume 2, pages 759–763, May 2004.

[13] Y. L. Chao and R. A. Scholtz. Optimal and suboptimal receivers for Ultra-Wideband transmitted reference systems. In *Proceedings of IEEE Global Communications Conference*, volume 2, pages 759–763, Dec. 2003.

[14] Y. L. Chao and R. A. Scholtz. Multiple access performance of Ultra-Wideband transmitted reference systems in multipath environments. In *Proceedings of IEEE Wireless Communications and Networking Conference*, pages 26–30, Mar. 2004.

[15] T. Jia and D. I. Kim. Analysis of average signal-to-interference-noise ratio for indoor UWB Rake receiving system. In *Proceedings of IEEE Vehicular Technology Conference*, volume 2, pages 1396–1400, May 2005.

[16] F. Tufvesson and A. F. Molisch. Ultra-Wideband communication using hybrid matched filter correlation receivers. In *Proceedings of IEEE Vehicular Technology Conference*, volume 3, pages 1290–1294, May 2004.

[17] S. Gezici, F. Tufvesson, and A. F. Molisch. On the performance of transmitted-reference impulse radio. In *Proceedings of IEEE Global Communications Conference*, volume 5, pages 2874–2879, Nov. 2004.

[18] L. Yang and G. B. Giannakis. Optimal pilot waveform assisted modulation for Ultrawideband communications. *IEEE Transactions on Wireless Communications*, Vol. 3(4):1236–1249, Jul. 2004.

[19] Z. Xu, B. M. Sadler, and J. Tang. Data detection for UWB transmitted reference systems with inter-pulse interference. In *Proceedings of IEEE International Conference on Acoustics, Speech, and Signal Processing*, volume 5, pages 2874–2879, Mar. 2005.

[20] D. I. Kim and T. Jia. M-ary orthogonal coded/balanced UWB transmitted-reference system. In *Proceedings of IEEE International Conference on Communications*, June 2006.

[21] B. Hu and N. C. Beaulieu. Accurate performance evaluation of time-hopping and direct-sequence UWB systems in multi-user interference. *IEEE Transactions on Communications*, Vol. 53(6):1053–1062, Jun. 2005.

[22] J. A. Gubner and K. Hao. An exact computable formula for the average bit-error probability of the IEEE 802.15.3a UWB channel model. In *Proceedings of IEEE Conference on Ultra-Wideband*, pages 142–146, Sep. 2005.

[23] X. Dong, A. C. Y. Lee, and L. Xiao. A new UWB dual pulse transmission and detection technique. In *Proceedings of IEEE International Conference on Communications*, volume 4, pages 2835–2839, May 2005.

[24] R. J. Fontana. A brief history of UWB communications. Multispectral Solutions Inc., Online available: http://www.multispectral.com.

[25] S. Roy, J. R. Foerster, V. S. Somayazulu, and D. G. Leeper. Ultrawideband radio design: The promise of high-speed, short-range wireless connectivity. *Proceedings of IEEE*, Vol. 92(2):295–311, Feb. 2004.

[26] J. D. Taylor. *Introduction to Ultra-Wideband radar systems.* CRC Press Inc., 1995.

[27] Revision of Part 15 the commission rules regarding Ultra-Wideband transmission systems. FCC, ET Docket 98-153, 2002.

[28] L. B. Michael, M. Ghavami, and R. Kohno. Multiple pulse generator for Ultra-Wideband communication using Hermite polynomial based orthogonal pulses. In *Proceedings of IEEE Conference on Ultra Wideband Systems and Technologies*, pages 47–51, May 2002.

[29] B. Parr, K. Wallace B. Cho, and Z. Ding. A novel Ultra-Wideband pulse design algorithm. *IEEE Communications Letters*, Vol. 7(5):219–221, May 2003.

[30] W. M. Lovelace and J. K. Townsend. The effects of timing jitter and tracking on the performance of impulse radio. *IEEE Journal on Selected Areas in Communications*, Vol. 20(9):1646–1651, Dec. 2002.

[31] S. Gezici, H. Kobayashi, H. V. Poor, and A. F. Molisch. The trade-off between processing gains of an impulse radio system in the presence of timing jitter. In *Proceedings of IEEE International Conference on Communications*, volume 6, pages 3596–3600, Jun. 2004.

[32] J. McCorkle. A tutorial on Ultrawideband technology. Online available: http://grouper.ieee.org/groups/802/15/pub/2000/Mar00/00082r1P802-15_WG–UWB–Tutorial–1–XtremeSpectrum.pdf, Mar. 2000.

[33] A. F. Molisch, J. R. Foerster, and M. Pendergrass. Channel models for Ultrawideband personal area networks. *IEEE Personal Communications Magazine*, Vol. 10(6):14–21, Dec. 2003.

[34] J. R. Foerster et al. Channel modeling sub-committee report final. IEEE P802.15-02/368r5-SG3a, Nov. 2002.

[35] G. L. Stüber. *Principles of mobile communication.* Kluwer Academic Publishers, 2001.

[36] J. M. Wozencraft and I. M. Jacobs. *Principles of Communication Engineering.* New York: John Wiley and Sons, Inc.,, 1965.

[37] A. Papoulis. *Probability, Random Variables, and Stochastic Processes.* New York, NY: McGraw-Hill, 1984.